July 2019

Studies on the Interaction and Organization of Bacterial Proteins on Membranes

Mariana Brena

Studies on the interaction and organization of bacterial proteins on membranes

A Thesis Presented

by

MARIANA BRENA

Submitted to the Graduate School of the
University of Massachusetts Amherst in partial fulfillment
of the requirements for the degree of

MASTER OF SCIENCE

May 2019
Molecular and Cellular Biology

Studies on the interaction and organization of bacterial proteins on membranes

A Thesis Presented

by

MARIANA BRENA

Approved as to style and content by:

_____
Alejandro P. Heuck, Chair

_____
Margaret Stratton, Member

_____
Min Chen, Member

_____
Scott C. Garman, Director
Molecular and Cellular Biology Program

ABSTRACT

STUDIES ON THE INTERACTION AND ORGANIZATION OF BACTERIAL PROTEINS ON MEMBRANES

MAY 2019

MARIANA BRENA, B.A., WELLESLEY COLLEGE

M.S., UNIVERSITY OF MASSACHUSETTS, AMHERST

Directed by: Professor Alejandro P. Heuck

Bacteria have developed various means of secreting proteins that can enter the host cell membrane. In this work I focus on two systems: cholesterol-dependent cytolysins and Type III Secretion.

Cholesterol is a molecule that is critical for physiological processes and cell membrane function. Not only can improper regulation lead to disease, but also the role cholesterol plays in cell function indicates it is an important molecule to understand. In response to this need, probes have been developed that detect cholesterol molecules in membranes. However, it has been recently shown that there is a need for probes that only respond to cholesterol that is accessible at the membrane surface. Perfringolysin O (PFO) is a toxin secreted by *Clostridium perfringens* that has been developed into a probe capable of detecting accessible cholesterol. Recently, researchers have been expanding the capabilities of this probe by substituting residues, modifying residues, truncating the probe, or a combination of the three. However, lack of characterization of these new probes has led to controversial results. To understand the role of a conserved Cys residue, here we perform cholesterol binding assays and measure the pore formation activity of a Cys modified PFO derivative.

The Type III Secretion (T3S) system is a syringe-like apparatus used by various pathogens to inject effector proteins into target cells. The apparatus spans both the inner and outer bacterial membrane, extending to make contact with the host cell where it forms a pore known as the translocon. In *Pseudomonas aeruginosa*, the translocon is made up of two proteins, PopB and PopD. While recent advances have been made on the structure of the needle and injectisome, information on the translocon remains sparse. In this work, the *P. aeruginosa* T3S translocon is analyzed using both *in vivo* and *in vitro* methods.

TABLE OF CONTENTS

Page

LIST OF TABLES

LIST OF FIGURES

Figure Page

CHAPTER 1

INTRODUCTION

1.1 Bacterial pathogens secrete proteins that assemble complexes on the target cell membrane

A common theme in bacterial pathogenesis is the need to communicate and interact with target cells. For this purpose, bacteria secrete proteins that bind, oligomerize, and form pores or channels in the plasma membrane of mammalian cells. For example, Gram-negative bacteria have dedicated secretion systems that span the bacterial membrane to secrete virulence factors (Costa et al 2015). Another common example of proteins secreted by bacteria that interact with host cell membranes include the family of pore forming toxins, which have a range of structures and pore forming mechanisms (Peraro and van der Goot 2016). In this work I will focus on two of these systems: the cholesterol-dependent cytolysins and the Type III Secretion system.

1.2 Cholesterol-dependent cytolysins: sensing cholesterol at the target membrane

1.2.1 Cholesterol

Cholesterol is an important molecule responsible for the proper structure and function of membranes (Maxfield 2010). In the membrane, the non-polar tail of cholesterol is oriented to interact with the hydrophobic chains of other lipids, while the hydroxyl group interacts with the head groups of other lipids (Figure 1.1). It is a hydrophobic molecule that can cross membranes, but the concentration within membranes is tightly controlled because changes in concentration can result in changes in

mammalian membrane structure (Maxfield 2010). Additionally, there are many proteins that sense, bind, and transport cholesterol, indicating the importance of cholesterol regulation (Maxfield 2010). Improper regulation of cholesterol can lead to diseases such as Niemman-Pick type C disease, Tangier disease, and atherosclerosis (Maxfield 2005). Due to the importance of proper cholesterol regulation, there is a need for probes to study cholesterol homeostasis and transport.

1.2.2 Perfringolysin O

Perfringolysin O (PFO) is a pore-forming toxin secreted by the Gram-positive pathogen *Clostridium perfringens*, and is part of a larger family of cholesterol-dependent, pore-forming toxins secreted by Gram-positive bacteria. It is classified as a cholesterol-dependent cytolysin (CDC) because it requires the presence of cholesterol in membranes in order to bind and form pores (Ohno-Iwashita 1992, Heuck et al 2000). When compared to PFO, many of the CDCs show an amino acid sequence identity greater than 39% (Heuck et al 2010).

1.2.3 PFO binding mechanism

Full-length PFO was arbitrarily divided into four different structural domains called domain 1 through 4 (Rossjohn 1997) (Fig 1.2). The PFO pore-formation mechanism can be described as follows: secreted as a 52.6 kDa water-soluble monomer, PFO first binds to cholesterol-containing membranes and oligomerizes with 35-40 other monomers to form a pre-pore complex. Lastly, PFO inserts β barrels to form a pore with a diameter of ~300Å in the target membrane (Fig. 1.3). The conformational changes required for PFO to insert into the membrane are initiated by the interaction between the distal loops found at the tip of the C-terminal domain, or domain 4 (D4), and the membrane (Ramachandran 2002). Upon D4 binding to the membrane, a conformational

A.

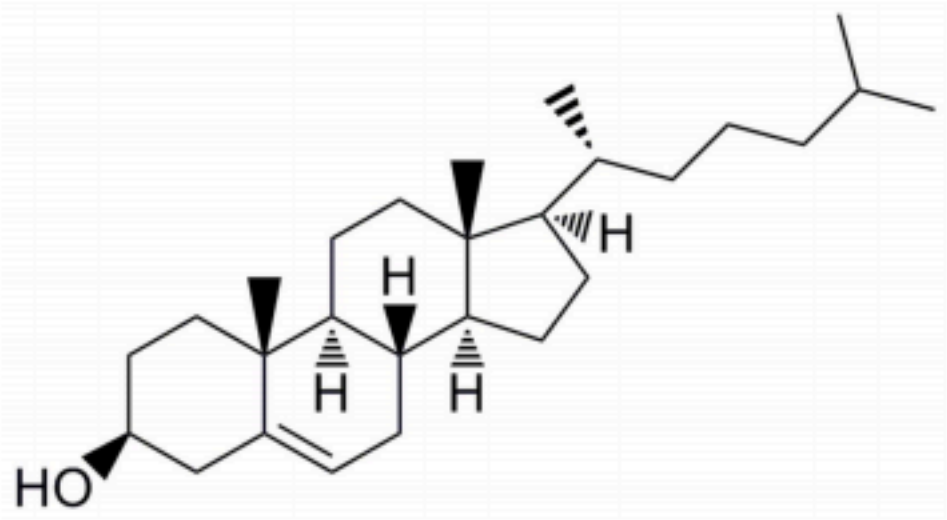

B.

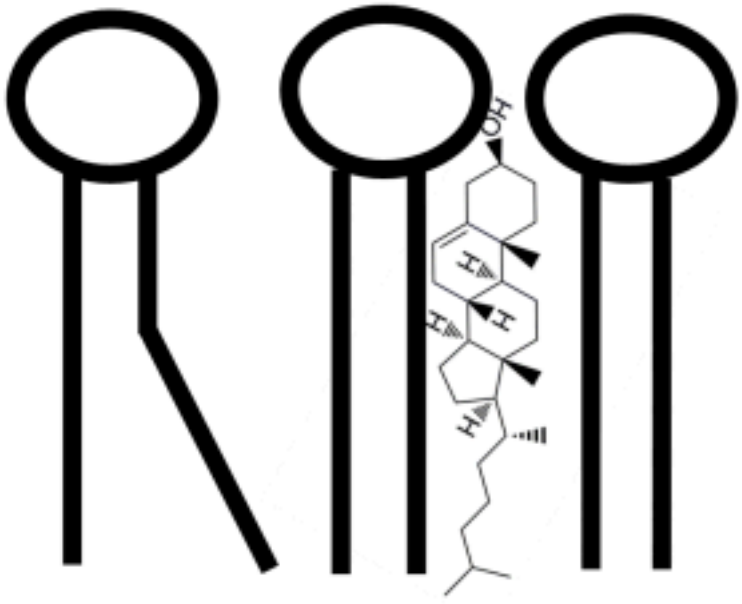

Figure 1.1 Cholesterol molecule and its orientation in the membrane. A. Depiction of the cholesterol molecule. B. The orientation in a membrane. Taken from Johnson 2014.

change causes domain 3 (D3) to expose a β strand required for monomer-monomer contact, which then leads to oligomerization and alignment to form a pre-pore complex (Ramachandran 2004). This pre-pore complex then guides the insertion of two β hairpins per monomer into the target membrane (Shepard 1998, Shatursky 1999), which ultimately results in pore formation (Hotze 2002). Interaction with cholesterol is critical during membrane binding because it is sufficient to trigger the formation of PFO ring-like complexes (Heuck 2007). Recently, it has become apparent that the interaction between PFO and cholesterol depends on how accessible cholesterol is at the membrane surface (Flanagan 2009, Johnson et al 2017).

1.2.4 Cholesterol accessibility

As previously mentioned, cholesterol is an important molecule for biological functions. Its interactions with other membrane components such as other lipids or molecules in the membrane dictate its ability to interact with molecules, such as PFO, at the surface of the membrane. For example, an increase in overall cholesterol concentration would result in more cholesterol exposed at the surface, or more accessible cholesterol (panel A, Fig. 1.3). Similarly, changes in the overall phospholipid composition will result in more or less cholesterol that is accessible at the membrane surface (panels B and C, Fig. 1.3).

Probes such as extrinsic fluorophores that bind to cholesterol or intrinsically fluorescent sterols that mimic cholesterol have been successfully used as fluorescent reporters to study intracellular cholesterol transport (Maxfield 2012). However, it has been reported that some regulatory events in the cell are modulated by the changes in the accessibility of cholesterol at the membrane surface (and not total cholesterol content)

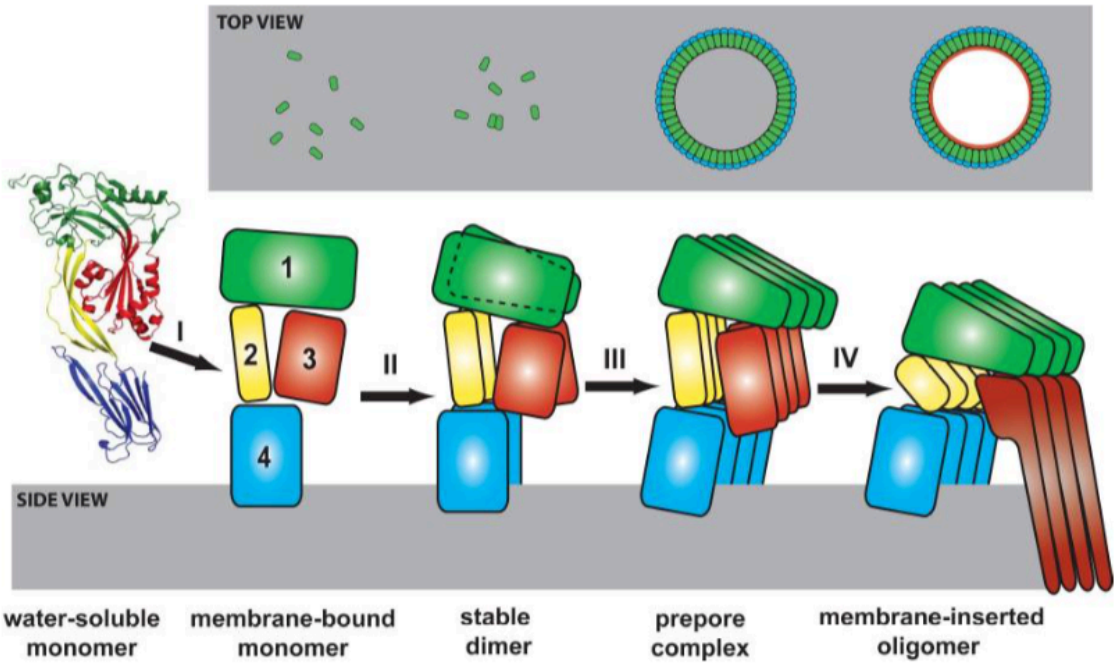

Figure 1.2 The pore formation steps of PFO. The ribbon structure of Perfringolysin O is shown on the left with the four different domains highlighted in different colors: Domain 1 is green, Domain 2 is yellow, Domain 3 is red, and Domain 4 is blue. The steps of the pore formation mechanism of PFO are illustrated as follows: PFO is secreted as a monomer before binding to a membrane (step I), where it then oligomerizes with other monomers (steps II and III) before inserting β hairpins to form a pore (step IV). Taken from Johnson 2014.

(Steck 2010). The aforementioned probes measure all cholesterol molecules and cannot detect changes in accessibility that could be triggered not only by changes in cholesterol concentration, but also by changes in the composition of other molecules in the membrane.

Given that significant changes in cholesterol accessibility could be triggered by small changes on the total cholesterol content or no changes at all (i.e., changes on other lipids that affect cholesterol accessibility) it is difficult to measure cholesterol accessibility and its changes using probes designed to measure total cholesterol. To address this challenge, biosensors have been developed that bind to membranes only when cholesterol is accessible at the surface. Because PFO only recognizes accessible cholesterol, in contrast to other probes that report total cholesterol content in membranes, PFO as a probe is better suited to measure cholesterol accessibility. Because it is used as a cholesterol probe, it is necessary to understand the interaction between PFO and cholesterol.

1.2.5 Domain 4 and cholesterol recognition

The region in D4 responsible for cholesterol recognition consists of four loops interconnected by β strands located at the distal tip of the domain: L1, L2, L3, and the undecapeptide. Across all 28 members of the CDC family, these loops, specifically the undecapeptide, are highly conserved (Savinov and Heuck 2017) (Figure 1.4). There is a proposed cholesterol binding motif located in L1 composed of two residues, T490 and L491, that are conserved throughout every known CDC (Farrand et al 2010). However, the substitution of residues in any of loops at the tip of D4 causes the cholesterol-binding threshold of

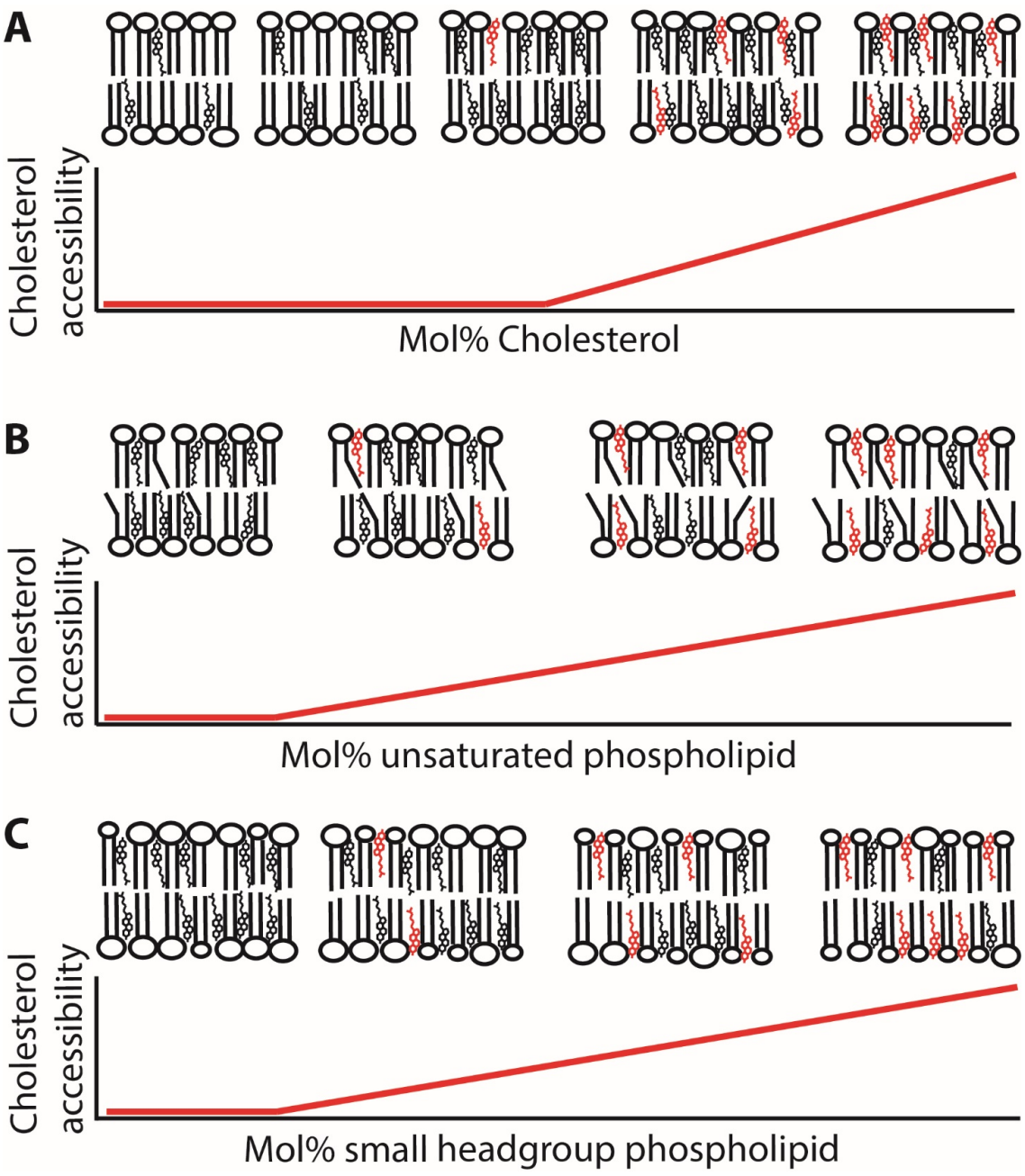

Figure 1.3 Cholesterol accessibility depends on lipid composition. A) When overall cholesterol content increases. B) When the number of double bonds on acyl chains of phospholipid changes. C) When phospholipid head groups are modified. Taken from Johnson 2014.

PFO derivatives to shift, indicating the importance of this domain in the process of cholesterol recognition (Johnson 2012). This is echoed by the induced fit model of cholesterol interaction created by Savinov and Heuck that shows interaction between the loops in D4 and a cholesterol molecule (Savinov and Heuck 2017). However, the exact residues responsible for cholesterol recognition are not yet known.

Despite the uncertainty, studies have been done on CDCs that demonstrate the importance of certain residues in pore formation. In CDCs such as Pneumolysin (PLY), substitution of the highly conserved Cys, which is located in the undecapeptide, with glycine or serine reduces the ability for the toxin to lyse polymorphonuclear leukocytes (Saunderst et al 1989). Additionally, substitution of other highly conserved residues near the Cys residue also causes reduced cell lysis (Korchev et al 1998). Early studies of other cytolysins such as Streptolysin O, found that the addition of N-ethyl maleimde inhibited lysis of red blood cells (Oberley and Duncan 1971). In full-length PFO, it has been demonstrated that modification of the highly conserved Cys459 with a thiol-blocking agent decreases the hemolytic activity of the protein, therefore inactivating the toxin (Iwamoto 1987). Removal of the thiol-blocking agent with DTT caused the toxin to gain function again. In other words, modification of Cys459 alters the ability of full-length PFO to bind cholesterol.

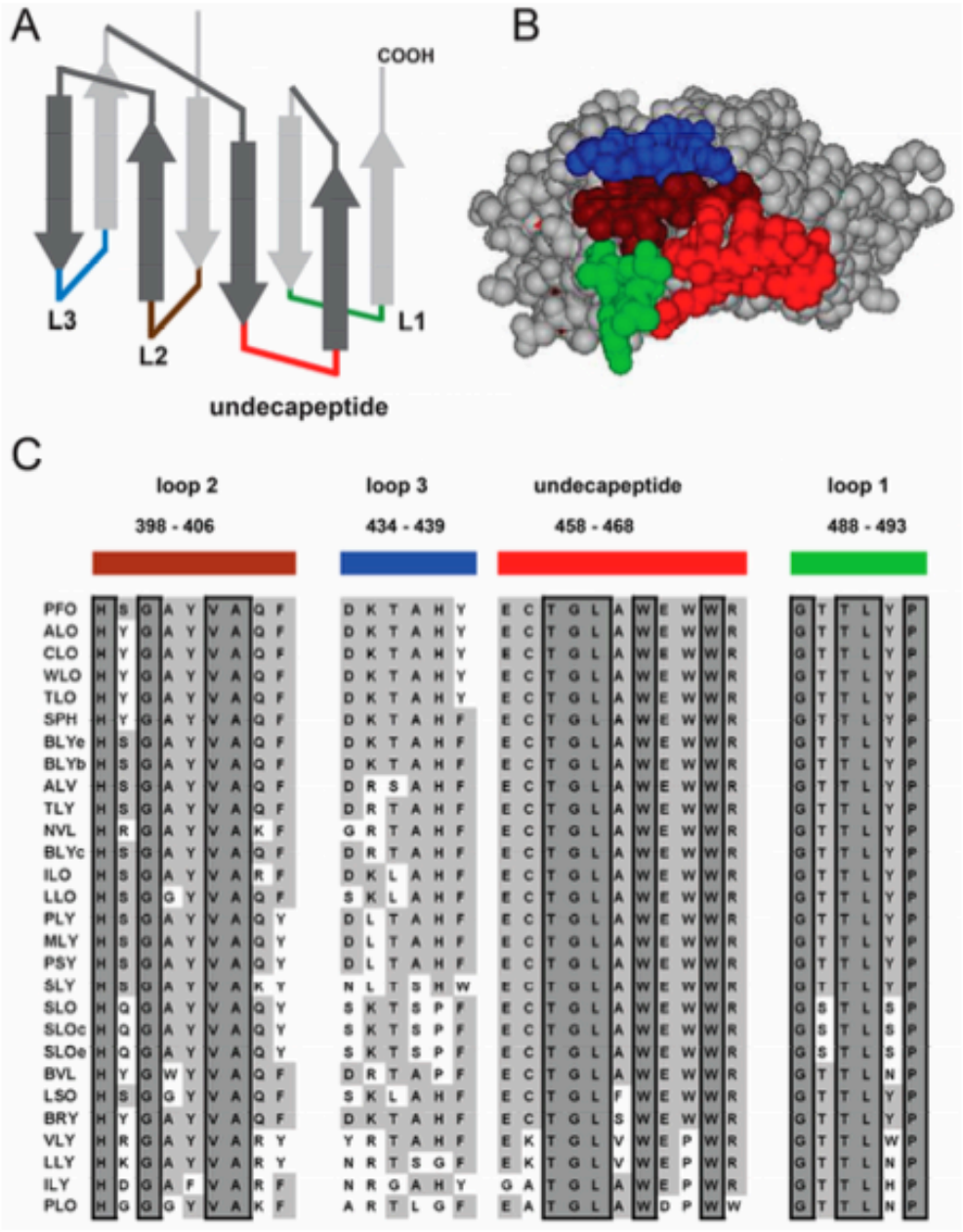

Figure 1.4 The loops at the tip of D4 are highly conserved among CDCs **A**) Cartoon representation the PFO D4 β-sandwich showing the location of the loops and the conserved undecapeptide.The undecapeptide was colored red and the loops were colored green (L1), brown (L2), and blue undecapeptide was colored red and the loops were colored green (L1), brown (L2), and blue (L3); (B) (L3); (**B**) A view of the tip of PFO D4 from the bottom showing the loops and undecapeptide color coded as in A; (**C**) Sequence alignment of the 28 CDC family members showing the conserved amino acids boxed and with dark grey background. Highly conserved amino acids are shown with a light grey background. Taken from Savinov and Heuck 2017.

1.2.6 PFO as a cholesterol probe

As mentioned previously, PFO is unique in that its binding is modulated by cholesterol accessibility. Based on these properties, researchers have created a series of cholesterol probes based on CDCs. By substituting amino acid residues in D4, it is possible to create probes with different cholesterol binding thresholds (Johnson 2012). Researchers have also been able to create a truncated probe that is non-lytic due to its inability to oligomerize by exploiting cholesterol-binding properties of the C-terminal domain, or D4 (Shimada 2002). The D4 of other CDC toxins has also been isolated and characterized, such as a CDC produced by *Bacillus anthracis*, anthrolysin O (ALO). Like PFO, ALO has also been shown to respond to cholesterol accessibility influenced by other lipids and not just total cholesterol concentration (Gay 2015). These D4 probes can also be further modified to alter the cholesterol threshold (Maekawa 2015) or by labeling cysteine residues with fluorophores (Gay 2015, Liu 2017). Because of the use of PFO as a cholesterol probe, a precise knowledge of how PFO recognizes cholesterol is required to properly use it as a cholesterol sensor.

Recently, lack of proper characterization has led to controversial results that are being debated in the literature. Liu et al reported that they were able to label the conserved Cys residue on isolated D4 with a fluorophore and lose sensitivity to lipid composition (Liu et al 2017). These surprising results spurred other researchers to study this labeled D4 probe more rigorously, where they were able to find that phospholipid composition does influence the binding of the D4 probe (Courtney et al 2018). Therefore, there is a need to characterize the effect of labeling the conserved Cys on D4.

1.3 The Type III secretion system

1.3.1 Type III Secretion

Another mechanism of bacterial virulence is the Type III Secretion (T3S) system. The T3S system is a multi-protein complex found in many Gram-negative bacteria and used to inject effector proteins into host cells (Hueck 1998). Resembling a syringe, the different components of the T3SS include a cytosolic platform, a basal body that traverses the inner and outer bacterial membrane, the needle that extends from the bacterial membrane to the host cell membrane, and a translocon complex through which the effector proteins are translocated into the host cell (Deng et al 2017). The needle structure has been visualized in pathogens such as *Y. enterocolitica* (Kudryashev et al 2013) *S. flexneri*, (Hu et al 2015) and *S. typhimurium* (Worrall et al 2016, Hu et al 2013, Park et al 2018).

As shown in Figure 1.5, the T3S system spans the inner and outer bacterial membrane, with the needle portion extending to make contact with the host cell membrane, where the translocon is formed. While cryo-electron microscopy (cryo EM) has served as a helpful tool to analyze the different components and stoichiometry of the T3S system, or injectisome, there is limited information on the translocon (Worrall et al 2016, Hu et al 2013). Further, there is limited structural information on the interaction between the needle tip and translocon, or the translocon and host membrane. Recently, more efforts have been made to understand the translocon. In contrast to the needle structures found by cryo EM, understanding of the translocon structure has been limited (Park et al 2018, Nauth et al 2018).

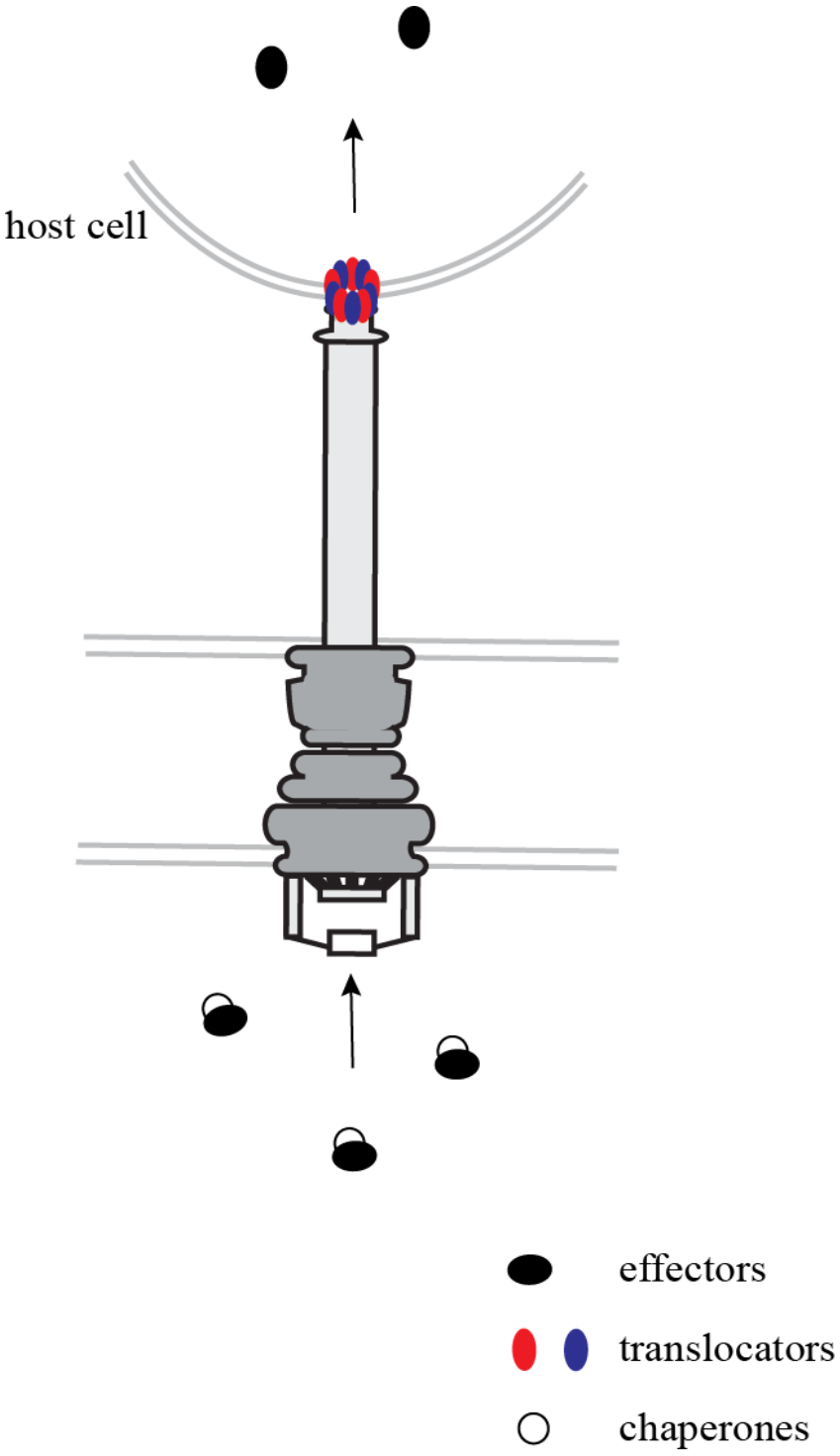

Figure 1.5 Schematic representation of *P.aeruginosa* needle and translocon.The structure of the T3S needle is shown in gray spanning the inner and outer membrane. The assembled translocon is depicted in blue and red, inserted on the host cell membrane.Effectors are shown in black with white chaperones. Image generated by Y. Tang

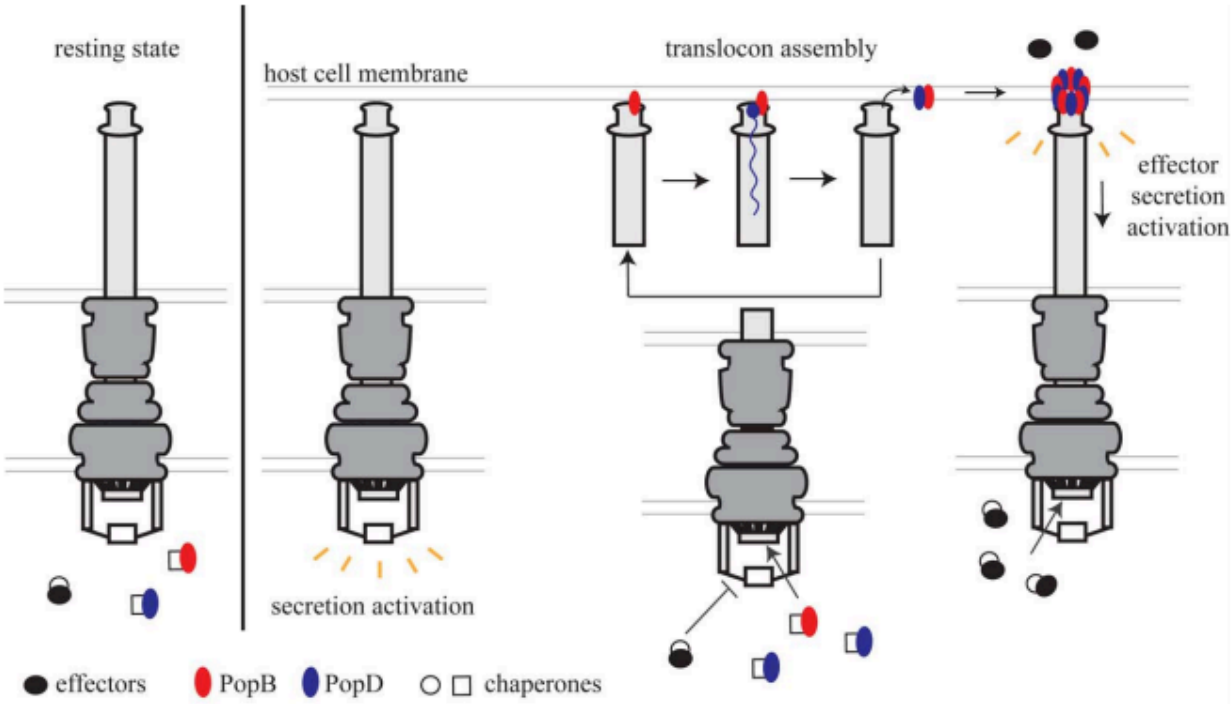

Figure 1.6 Hypothetical schematic of T3S system translocon formation and effector secretion. Upon activation, the needle secretes the translocators, PopB and PopD, either alternately or stochastically. They then assemble on the host cell membrane and secretion of effectors commences. Taken from Vermeulen et al 2016.

Upon contact with the host cell membrane, the T3S system is activated to secret effector proteins into the host cell (Pettersson et al 1996) (Fig. 1.6). Secretion can also be induced under low-calcium conditions (Goure 2004, Vallis 1999). Prior to injection of effector proteins into the host cell, the translocon must be assembled.

1.3.2 *Pseudomonas aeruginosa* translocon

In *Pseudomonas aeruginosa*, the translocon is formed by two proteins, PopB and PopD, 40 kDa and 31 kDa respecively. Upon T3S system activation, PopB and PopD are secreted and inserted into the host cell membrane through which *Pseudomonas* effectors ExoS, ExoT, ExoY, and ExoU are translocated into the host cell. Both PopB and PopD are required for effector translocation (Romano et al 2016). Without either translocator present, *P. aeruginosa* is unable to successfully translocate proteins into host cells (Goure 2004). Unlike the injectisome, which has been visualized in other Gram-negative pathogens mentioned above, the translocon has yet to be visualized. The only structure available relating to the proteins that form the translocon is the crystal structure of PopB homologue, AopB, from *Aeromonas hydrophila* in complex with its chaperone, AcrH (Nguyen et al 2015).

While the structure of the injectisome of the Type III Secretion system has been characterized in some Gram-negative pathogens, visualization of the translocon remains a challenge. Specifically, due to the non-polar nature of PopB and PopD, their interactions with the membrane, and the hetero-oligomeric organization, have been difficult to visualize. Nonetheless, important information on the assembly and orientation of the translocators has been discovered through biochemical analysis (Tang et al 2018). These studies are important because they help to model the arrangement of PopB and PopD in

the membrane and assist in our understanding on how they interact with each other and the needle. This knowledge could then be used to identify methods of disrupting the translocon and ultimately, *P. aeruginosa* infection.

In *P. aeruginosa*, the conditions to maximize translocon heterocomplex formation on model membranes have been previously established (Romano 2011), and by using single molecule analysis and fluorescence photobleaching, these membrane integral proteins have been found to assemble a heterocomplex with a distinct stoichiometry of 8 subunits of PopB and 8 subunits of PopD (Romano 2016). More recent biochemical analysis of the translocon has shown that PopB assists the insertion of PopD into the host cell membrane (Tang et al 2018). Despite these advances, there is still a lack of information on the topology of the translocators in the membrane.

CHAPTER 2

CHARACTERIZATION OF THE PERFRINGOLYSIN O CHOLESTEROL-DEPENDENT BINDING WHEN THE CONSERVED CYS459 RESIDUE IS MODIFIED WITH COVALENTLY ATTACHED GROUPS

2.1 Introduction

Modifications to the loops at the tip of PFO D4 alter the affinity of PFO for cholesterol-containing membranes (Johnson 2012). Within one of these loops, the undecapeptide, there is a unique Cys459 that can be used to specifically introduce groups with different chemical characteristics. The introduction of these different groups can be used to study the forces that regulate PFO binding to membranes. While modifications to this Cys have been reported to be detrimental for protein hemolytic activity (Iwamoto et al 1987), recent results suggested that modifications to the Cys might alter the cholesterol dependent binding of PFO (Liu et al 2017). Here, we covalently attach fluorescent probes to the conserved Cys459 and measure the impact this modification has on the cholesterol binding and pore formation mechanism of PFO.

2.2 Results

In order further characterize which steps of the PFO mechanism, if any, are altered by modifying the conserved Cys, independent assays that measure binding, pore formation *in vivo* and *in vitro* were used. To see if modifying this residue causes full-length PFO to lose sensitivity to lipid composition, as suggested by Liu et al, we modified the conserved Cys residue with two different fluorophores. We used two

probes, acrylodan or NBD, to modify Cys459 on wtPFO. Acrylodan is a hydrophobic fluorophore and was used by Liu et al in their studies. We also chose to label the conserved Cys with NBD because it is more polar than acrylodan, and it has a lower tendency to locate into the membrane. The effect of the fluorophore on PFO derivatives was then characterized by independently measuring their cholesterol binding threshold, the effect of lipid composition, their hemolytic activity, and their pore formation activity in model membranes, and the results were compared to wtPFO.

2.2.1 Cholesterol binding

PFO contains 6 of the 7 native tryptophan (Trp) residues in D4, which allows us to directly monitor binding using intrinsic Trp emission. When PFO binds to membranes, these Trp residues locate into a non-polar environment, which causes them to display an increase in fluorescence when compared to the polar environment sensed by these residues when PFO is monomeric in an aqueous solution. A sharp increase in the intrinsic fluorescence of PFO is observed in a relatively narrow range of cholesterol concentration (~4 mol%) when PFO is incubated with liposomes containing increasing amounts of cholesterol. The cholesterol concentration that produces 50% binding of PFO is defined as the cholesterol binding threshold. For wtPFO, the cholesterol threshold was determined by Johnson et al by quantifying cholesterol concentration and phospholipid concentration in liposomes containing 1:1:1 molar ratio of POPC, POPE, and SM (Figure 2.1) (Johnson et al 2012). Based on this quantification, wtPFO can be used as a reliable reference. Liposomes containing 30-50 mol% cholesterol and a 1:1:1 molar ratio of POPE:POPC:SM were prepared and the cholesterol binding threshold was determined by incubating liposomes with labeled and unlabeled PFO and measuring the resulting increase in the dye fluorescence or intrinsic fluorescence as a function of cholesterol

concentrations, respectively. The introduction of a modification on Cys459 did not seem to significantly alter the cholesterol binding threshold, although the fluorophore-labeled PFO derivatives did not have as sharp a response as wtPFO (Figure 2.2).

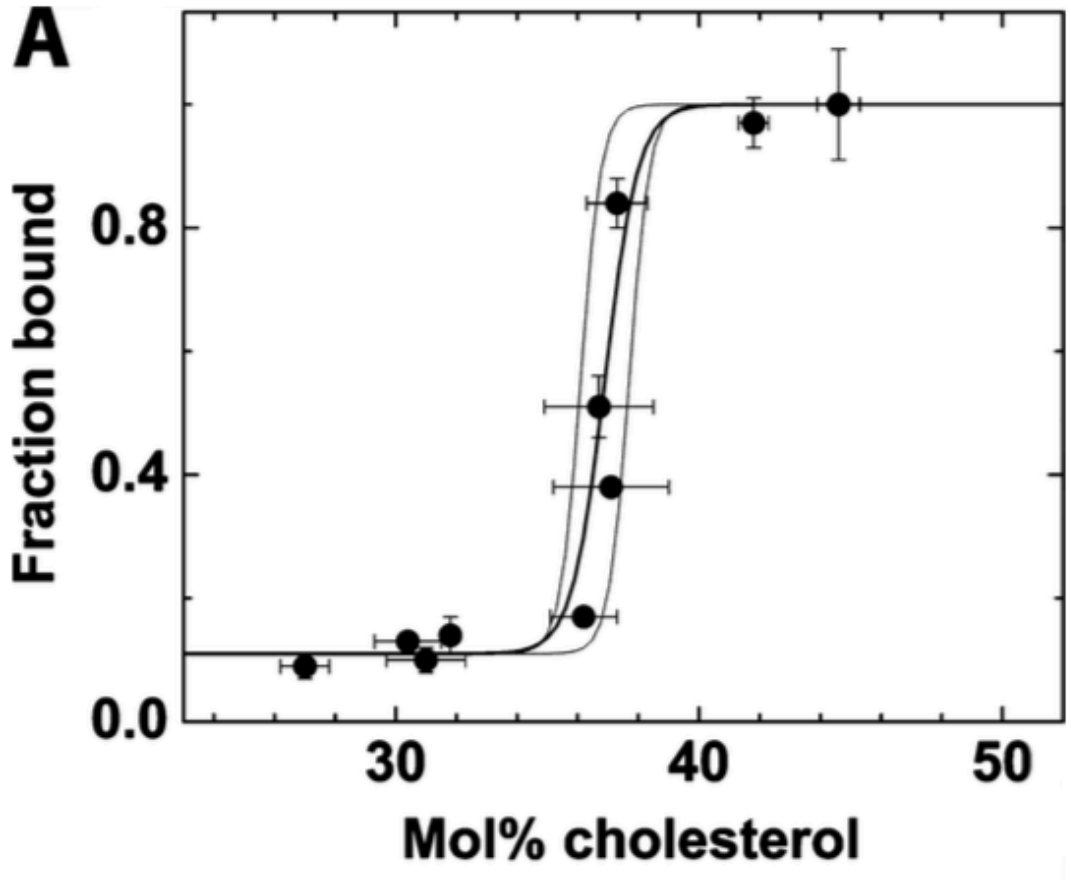

Figure 2.1 Determination of the cholesterol threshold for nPFO (final concentration of 200 nM) on POPC/POPE/SM membranes containing the indicated mole percent of cholesterol (final total lipid concentration of 100 μM). The mole percent of cholesterol was determined by individual quantification of cholesterol and total phospholipids. Cholesterol was quantified using Amplex Red, and total phospholipids were quantified by phosphate determination after acid hydrolysis as described in Experimental Procedures. Thin lines are a guide for the eye to indicate the average range for data in the transition. Taken from Johnson et al 2012.

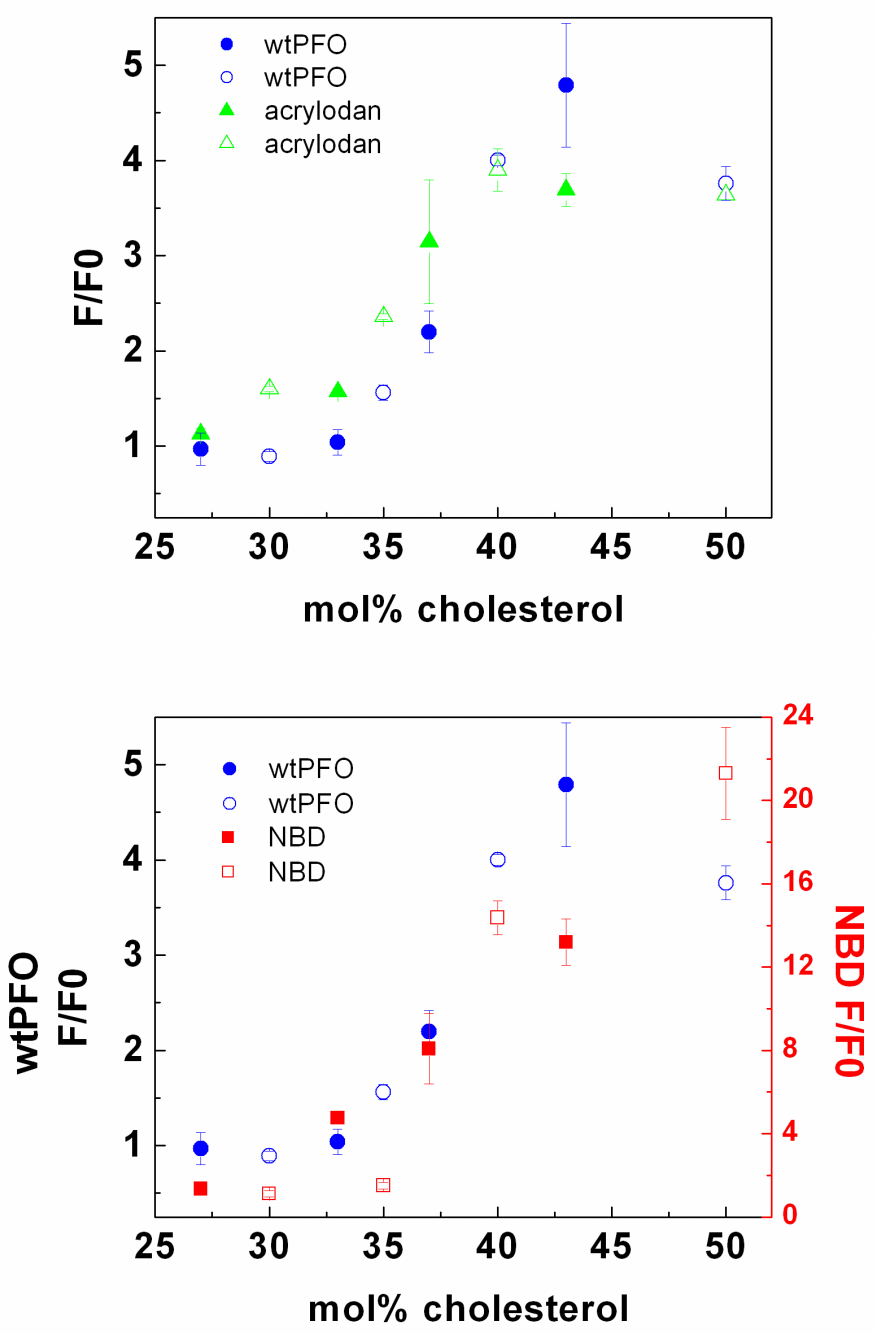

Figure 2.2. Modification of Cys459 does not significantly alter chol binding in liposomes. Proteins were incubated with two different set of liposomes (open and closed symbols) containing a 1:1:1 ratio of POPC:POPE:SM and the indicated cholesterol concentration for 20 min at 37 ˚C. The final fluorescence, F, was divided by the initial fluorescence, F_0. Final protein concentration was either 200 nM for NBD-labeled PFO and wtPFO or 160 nM for acrylodan-labeled PFO. The final lipid concentration was 200 µM. Acrylodan labeling was 100% (Batch 1) and NBD labeling was 81% (Batch 1).

2.2.2 Lipid sensitivity

In order to observe how the lipid composition affects the cholesterol-dependent binding of Cys-labeled PFO, liposomes containing 20-50 mol% cholesterol and DOPC were prepared and incubated with wtPFO and labeled PFO. Compared to the lipid composition used in Fig. 2.2, this lipid composition will contain more unsaturated acyl chains. More unsaturated acyl chains will decrease the amount of cholesterol required to trigger PFO binding (Flanagan et al 2009). This should lead to a lower cholesterol binding threshold when compared to the one obtained using liposomes with a 1:1:1 SM:POPE:POPC lipid composition. As expected, there was a lower cholesterol binding threshold for wtPFO (solid blue circles compared to open blue circles, Figure 2.3). Additionally, the labeled PFO derivatives exhibited a shift in cholesterol binding threshold (green and red symbols, Figure 2.3). However, while the profile for NBD-labeled PFO was similar to the binding curve for wtPFO (right panel, Figure 2.3), the profile for acrylodan-labeled PFO was different from wtPFO (left panel, Figure 2.3). The threshold for acrylodan-labeled PFO decreased from approximately 35 mol% cholesterol to 15 mol% cholesterol (left panel, Fig. 2.3).

2.2.3 Pore formation

While measuring intrinsic Trp emission is indicative of PFO binding, measuring pore formation is indicative of the ability for PFO to oligomerize and insert the transmembrane β barrels. In order to measure pore formation, liposomes containing the fluorescent complex $Tb(DPA)_3^{3-}$ were prepared with a high cholesterol concentration (50 mol%). The binding reaction was carried out in buffer containing the membrane-impermeable EDTA, which chelates Tb^{3+} and quenches its emission. When pores are

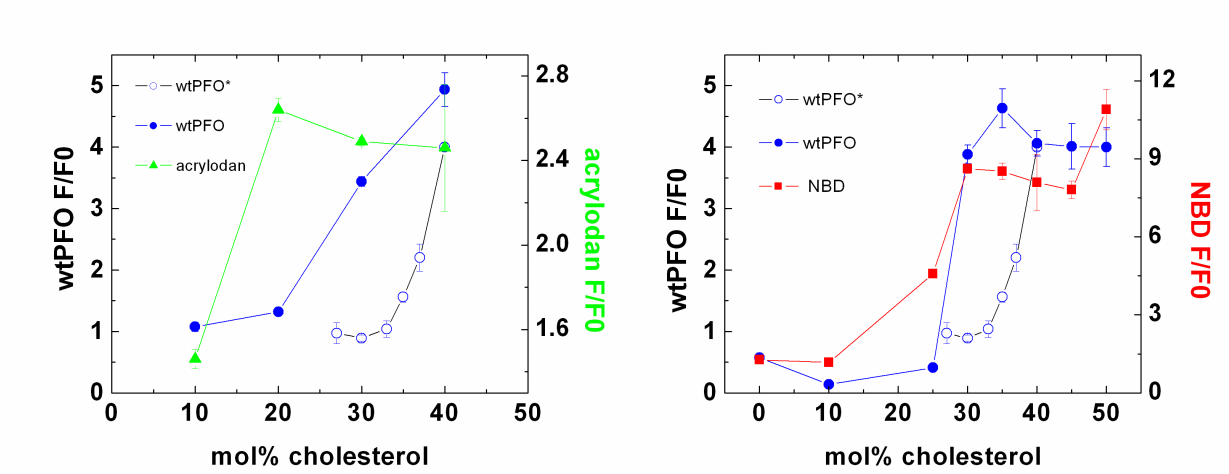

Figure 2.3 Labeled and unlabeled PFO is sensitive to lipid composition. Liposomes (200 µM final concentration) containing DOPC and the indicated cholesterol concentration were incubated with either 200 nM wtPFO or NBD-labeled PFO or 160 nM acrylodan-labeled PFO for 20 min at 37 ˚C. The emission after liposomes incubation (F) was divided by emission for monomeric PFO before addition of the liposomes (F_0). NBD labeling was 92% (Batch 2) and acrylodan labeling was 100% (Batch 4).

formed in the liposomes, EDTA is able to access the encapsulated $Tb(DPA)_3^{3-}$ complexes. Therefore, a decrease in fluorescence correlates to pore formation. As seen in Figure 2.2, a cholesterol concentration of 50 mol% results in both wtPFO and labeled PFO being maximally bound to the membranes. Therefore, we used this cholesterol concentration to ensure maximum PFO binding. As with wtPFO, both labeled PFO derivatives tested were able to form pores in liposomes. However, in contrast to similar thresholds in the cholesterol binding assays, the labeled PFO derivatives showed slightly lower pore formation activity when compared to wtPFO (Figure 2.4). The protein concentration-dependent quenching of wtPFO parallels the one observed for NBD-labeled PFO. Acrylodan-labeled PFO showed lower pore formation activity and plateaued above 100 nM protein (Figure 2.4). While more experiments will be required to explain the small differences observed for the acrylodan-labeled PFO and the wtPFO, it is clear that the three proteins were able to perforate the liposomal membrane and form pores.

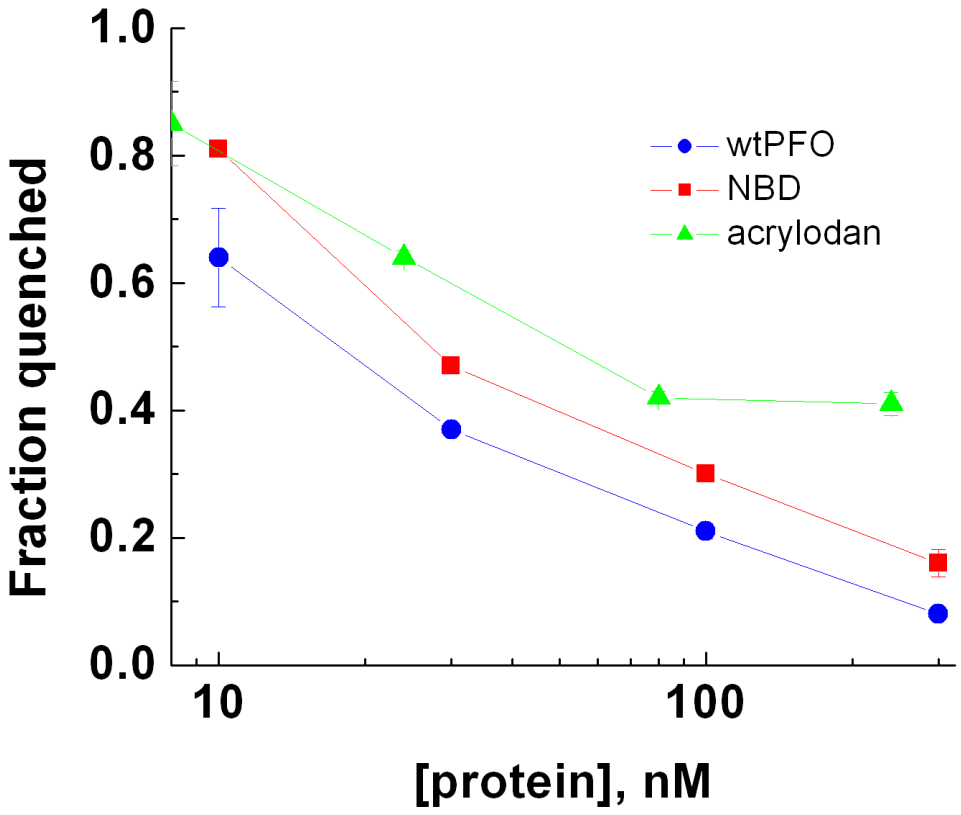

Figure 2.4 NBD and acrylodan-labeled PFO can form pores in cholesterol-containing liposomes. Liposomes with a high percentage of cholesterol (50 mol%) were prepared containing $Tb(DPA)_3^{3-}$ ions. Fluorescence was measured before and after incubation with the indicated protein. The average of two experiments are shown with error bars indicating range. Acrylodan-labeled PFO was 100% labeled (Batch 3) and NBD-labeled was 92% labeled (Batch 2).

2.2.4 Hemolysis

While cholesterol binding and pore formation are measured using model membranes, or liposomes, red blood cells (RBCs) can also be used to measure PFO-membrane interactions with more complex natural membranes. In order to accomplish this, RBCs were incubated with wtPFO or labeled-PFO for 20 minutes at 37 ˚C. The resulting lysis of the RBCs was measured by pelleting RBCs and measuring the hemoglobin released into the supernatant.

Both fluorophore-modified PFO derivatives were able to lyse RBCs at concentrations above 10 nM, however, NBD-labeled PFO required a ten-fold increase of protein to reach 50% hemolysis when compared to wtPFO (Figure 2.5). Acrylodan-labeled PFO showed an intermediate concentration-dependent response. These results confirmed that despite the small differences observed for the lytic activity of the Cys459-labeled PFO derivatives, all of them were able to form pores in model and natural membranes.

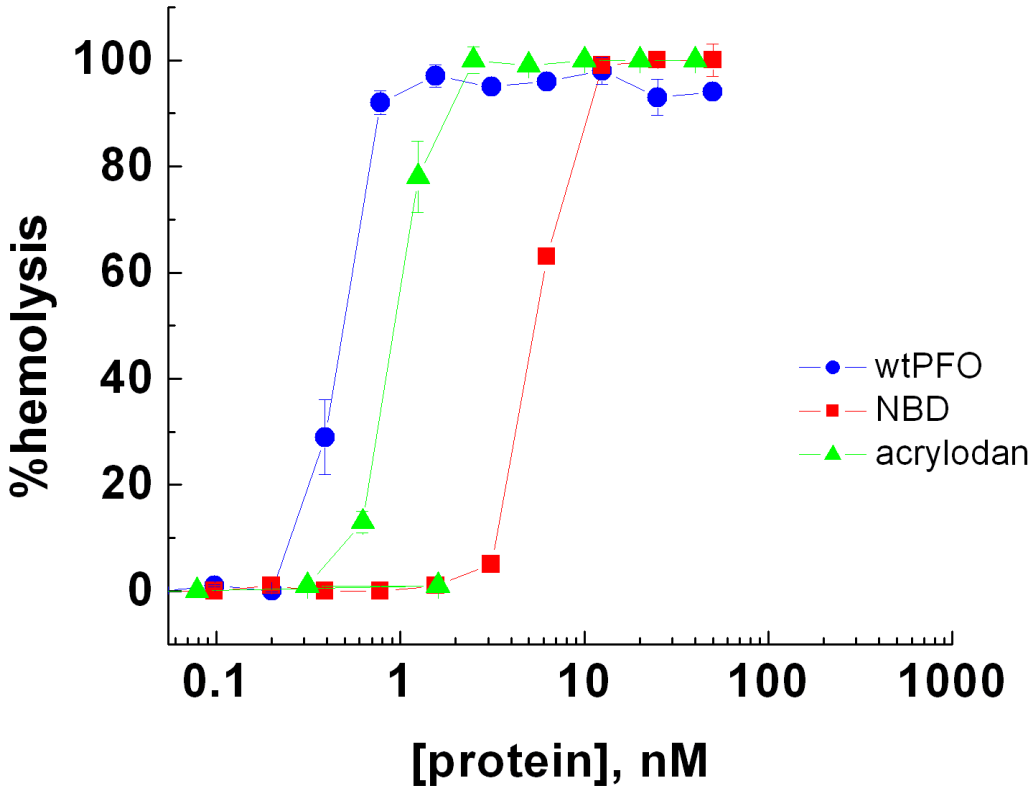

Figure 2.5. NBD-labeled PFO requires 10-fold higher concentration of protein to lyse red blood cells. Washed red blood cells were incubated with the indicated concentration of protein for 20 min at 37 ˚C. Hemoglobin release was recorded by pelleting cells and measuring absorbance at 540 nm using a plate reader. The average of two experiments is shown with error bars indicating range. Acrylodan labeling was 100% (Batch 3) and NBD labeling was 81% efficient (Batch 1).

2.3 Discussion

Wild-type PFO contains a unique Cys located in one of the loops at the tip of the D4 β -sandwich. This Cys was labeled with either the fluorophores IANBD (NBD) or acrylodan, and the properties of labeled PFO derivatives were compared to wtPFO (unlabeled protein) by measuring ability to bind to cholesterol-containing membranes and form pores. The cholesterol binding threshold was not significantly affected by covalent modification with these fluorescent dyes. Additionally, we measured pore formation ability to determine if the modified PFO can oligomerize and insert the β-barrel pore and found that the labeled PFO derivatives had slightly lowered pore formation activity, but were still able to form pores in cholesterol containing liposomes. Lastly, we measured the hemolytic activity of wtPFO and its labeled derivatives to demonstrate if the Cys-labeling affects lysis of natural cholesterol-containing membranes, finding that both derivatives were able to lyse red blood cells albeit requiring 10-fold more protein in the case of NBD-labeled PFO and a slightly higher concentration of acrylodan-labeled PFO.

Because of the results reported in Liu et al (2017), we chose to use acrylodan as one of our fluorophores. In addition to acrylodan, we used NBD, which is less hydrophobic than acrylodan, to observe the effect of hydrophobicity on the Cys residue. Our results show that modification with NBD and acrylodan to the conserved Cys residue in PFO does not significantly alter the cholesterol binding threshold (Figure 2.2) nor does it cause PFO to lose lipid sensitivity (Figure 2.3). However, it appears that pore formation in liposomes and red blood cells for labeled-PFO derivatives is not as efficient as wtPFO.

Previous studies have found that substituting the native Cys residue for an alanine residue causes an increased shift in the cholesterol binding threshold of 4 mol% cholesterol (Moe and Heuck 2010). Therefore, we expected to see an increase in the

cholesterol binding threshold when comparing Cys-modified PFO to wtPFO. It was surprising to see that there was not a significant difference in the cholesterol binding threshold between labeled and unlabeled PFO. However, it did appear that labeling PFO with a fluorophore caused the loss of the sharp response to an increase in the mol% cholesterol typically seen in wtPFO. In wtPFO, the binding threshold typically begins at around 36 mol% cholesterol and ends at approximately 40 mol% in liposomes containing the indicated cholesterol concentration and a 1:1:1 ratio of SM:POPE:POPC (Figure 2.1, Johnson et al 2012, 2017). This sigmoidal curve was replicated here, (blue circles in Figure 2.2), but a similarly sharp curve was not seen for acrylodan-labeled PFO or NBD-labeled (Figure 2.2). There was still a response to the increase in cholesterol, but the threshold was not as narrow as it is for wtPFO. This is likely due to the modification of Cys459. D4 is the first domain of PFO that comes into contact with membranes and if the conserved Cys or other residues in D4 are modified, there is a clear shift in the cholesterol binding threshold to higher cholesterol concentrations (Johnson et al 2012). Therefore, the addition of a fluorophore to D4 may explain the "extension" of the sigmoidal curve. Additionally, when measuring the cholesterol binding thresholds for PFO and the labeled derivatives, we are measuring fluorescence as the environment of either Trp or the fluorophore changes. It is possible that acrylodan and NBD emission is more affected by cholesterol concentration than Trp residues are. This could explain why there are variations in F/F0 at high cholesterol concentrations even though maximum binding has been reached for wtPFO and may explain why the cholesterol binding curve for the labeled PFO derivatives is flatter than the curve for wtPFO.

In contrast to the acrylodan-labeled D4 probe used by Liu et al, we did not find that labeling full-length PFO with NBD or acrylodan causes a loss of lipid sensitivity (Figure 2.3). To test this, the cholesterol binding curve for PFO and liposomes containing cholesterol and DOPC was measured using increase in Trp or fluorophore fluorescence as a guide for membrane binding. As expected for the DOPC liposome binding curve, the 1:1:1 SM:POPC:POPE liposome curve, shifted towards lower cholesterol concentration for wtPFO, NBD-labeled PFO, and acrylodan-labeled PFO. These results are in agreement with previous findings on the sensitivity of PFO to lipid composition (Flanagan 2009, Johnson et al 2017).

In the two assays that measure the ability for PFO to form pores, pore formation in liposomes and hemolytic activity, the labeled PFO derivatives were less able to form pores than wtPFO (Figure 2.4 and 2.5). This may be because while the modification on D4 does not impede cholesterol recognition, however it may affect the downstream conformational changes required for oligomerization and insertion of the β hairpins. During the binding mechanism, dimer formation causes conformational changes which then leads to oligomerization (Ramachandran 2004). The addition of a bulky molecule on Cys459 may impact dimerization or oligomerization, which would also explain the lowered hemolytic activity and pore formation activity in the labeled PFO derivatives.

Acrylodan-labeled PFO was able to lyse RBCs more efficiently than NBD-labeled PFO. This was in contrast to the pore formation results, which showed that NBD-labeled PFO formed more pores than acrylodan-labeled. This may be explained by the use of different samples for the two experiments. Both of these assays used the same batch of acrylodan-labeled PFO (Batch 3) but a different batch of NBD-labeled PFO with

different labeling efficiencies. In the pore formation assay, PFO was labeled with NBD with an efficiency of 92%, while in the hemolytic activity assay, the labeling efficiency was 81%. The presence of two different populations, labeled and unlabeled protein, mean that in addition to observing the interaction between the protein and the membranes, we observe the interaction between labeled and unlabeled protein. It was previously shown that mixing functional PFO with a PFO derivative that is unable to insert the β hairpins due to a Y181A substitution will induce the insertion of the β hairpins on the Y181A derivatives (Hotze et al 2002). Given our results, we may be observing two different populations at play: an unlabeled and a labeled population. Additionally, while the binding assay was normalized by the initial concentration of protein (F_0), the differences observed in these pore formation assays could originate in small differences in the calculated concentration of the proteins (despite the efforts to correct for the fluorescence contribution of acrylodan and NBD to the absorbance at 280 nm).

It has been established that during pore formation, D4 and D3 are conformationally linked (Heuck et al 2000). Additionally, D4 binding to the membrane is the switch that causes the conformational changes necessary for pore formation (Heuck et al 2007). It is therefore possible that modifications to the Cys459 in D4 can contribute to a decreased ability to form pores in membranes. While there was no significant difference in terms of cholesterol binding threshold, we did see that labeling PFO on the conserved Cys does not impair its ability to react to changes in cholesterol accessibility.

Given these results, it would be surprising that labeling Cys459 would cause a truncated D4 probe to lose lipid sensitivity. However, more studies are necessary to understand the mechanism behind cholesterol recognition and pore formation in PFO.

2.4 Materials and methods

2.4.1 Protein overexpression and purification

As reported previously in Flanagan et al 2009. The concentration of protein was estimated by measuring absorbance at 280nm and using a molar absorption coefficient of 74,260 $M^{-1}cm^{-1}$. Protein was stored with 10% glycerol and 5mM DTT at -80˚C after being flash frozen with liquid nitrogen.

2.4.2 Fluorophore preparation

Using a glass pipet, a small amount of fluorophore (N,N'-Dimethyl-N-(Iodoacetyl)-N'-(7-Nitrobenz-2-Oxa-1,3-Diazol-4-yl)Ethylenediamine (IANBD amide, Invitrogen) or 6-Acryloyl-2-Dimethylaminonaphthalene, (acrylodan, Thermo Fisher) was added to 100µL DMSO. The fluorophore was dissolved thoroughly before being centrifuged for 5 min at 16000 x g to remove any insoluble material. The supernatant was transferred to a new tube and a 1:500 dilution was prepared using spectroscopic grade methanol. To determine the concentration of the sample, the concentration of the fluorophore was determined by measuring the absorbance at 502nm for NBD or 372nm for acrylodan and using the molar absorptivities of 25,000 $M^{-1}cm^{-1}$ for NBD or 16,400 $M^{-1}cm^{-1}$ for acrylodan in methanol (Molecular probes catalogue).

2.4.3 Fluorophore labeling of native Cys residue

Purified wtPFO was loaded onto a column packed with Sephadex G-25 resin (GE Healthcare) and pre-equilibrated with 50 mM Hepes pH 8.3, 100 mM NaCl (HBS pH 8.3) to remove DTT. Protein was collected in 20-drop fractions and concentration was measured using absorbance at 280 nm. A final concentration of 3 M guanidine hydrochloride crystals were added to pooled peak fractions of protein. This sample was then incubated in a 1:10 molar excess of fluorophore for two hours with gentle rocking.

To remove excess fluorophore and guanidine hydrochloride, labeled protein was loaded on to a second Sephadex G-25 column equilibrated with 50 mM Hepes pH 7.5, 100 mM NaCl. Peak fractions were collected and the concentration of the fluorophore and protein was determined. Labeling efficiency was calculated by dividing the concentration of the fluorophore by the concentration of PFO by using the molar absorptivities of 25,000 $M^{-1}cm^{-1}$ for NBD, 16,400 $M^{-1}cm^{-1}$ for acrylodan, and 74,260 $M^{-1}cm^{-1}$ for PFO. To account for fluorophore contribution to absorbance of the protein, the absorbance of the fluorophore alone was measured at both the wavelength used to measure the fluorophore and at 280 nm. The absorbance contribution of the fluorophore to the absorbance of protein at 280 nm was calculated as follows: for NBD, $Abs_{280}/ Abs_{502} = 0.05$ and for acrylodan, $Abs_{280}/ Abs_{372} = 0.2$. Therefore, to determine the concentration of PFO for NBD-labeled PFO, 5% of the absorbance at 502 nm was subtracted from the protein absorbance while 20% of the absorbance at 372 nm was subtracted from the protein absorbance for acrylodan-labeled PFO. The chemical reaction that takes place between the fluorophore and the cysteine is shown in Figure 2.6.

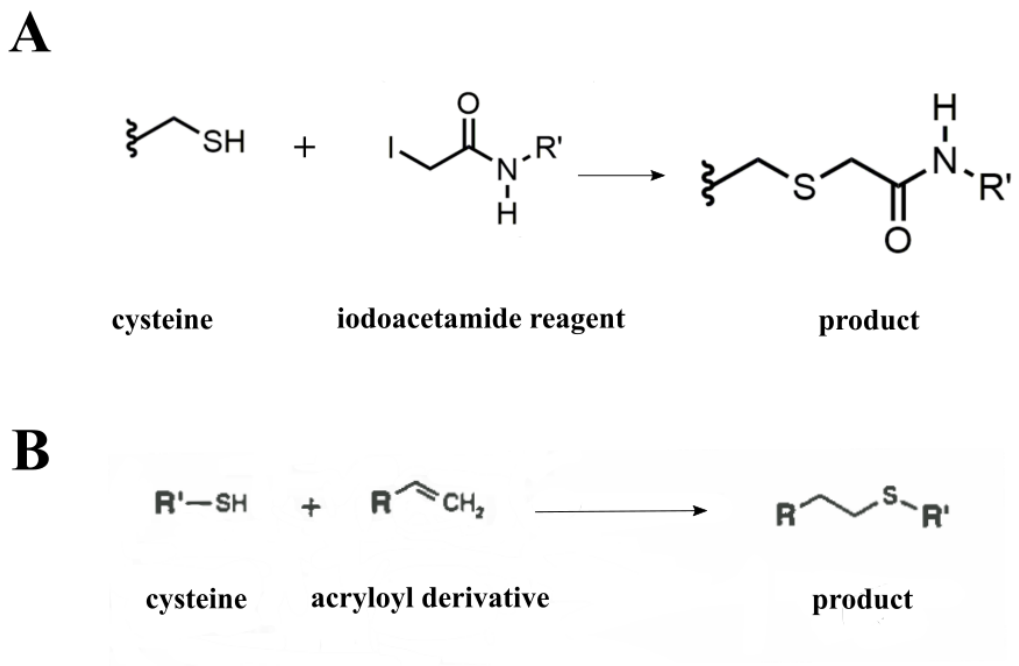

Figure 2.6 Fluorophore conjugation with sulfhydryl group on cysteine. (A) The reaction between IANBD and the conserved cysteine takes place between the iodoacetamide group on NBD and the sulfhydryl group on the cysteine. (B) The reaction between acrylodan (represented by the acryloyl derivative) and the sulfhydryl group.

2.4.4 Preparation of liposomes

All lipids except cholesterol (Steraloids) were from Avanti Polar Lipids. Lipids are stored dissolved in chloroform. The desired lipid composition was mixed well in a glass tube before the chloroform was evaporated using a gentle stream of nitrogen gas to form a lipid film on the bottom of the glass tube. The lipid films were further dried in a SpeedVac for 3 hours and then stored at -20˚C until the lipid film was resuspended in buffer containing 50mM Hepes pH 7.5 and 100mM NaCl (HBS pH 7.5) at 20-23 ˚C for 45 minutes. The resuspended lipids were then subjected to three freezing (-80˚C) and thawing (37˚C) cycles, each freeze or thaw step lasting 5 minutes. After the final thawing step, the lipids were passed through an extruder with a 0.1 μm membrane 21 times to form large unilamellar vesicles (liposomes). The liposomes were stored on ice at 4˚C for up to two weeks.

2.4.5 Preparation of liposomes containing $Tb(DPA)_3^{3-}$

Lipids dissolved in chloroform were mixed containing a 1:1:1 mol% ratio of sphingomyelin (SM), 1-palmitoyl-2-oleoyl-glycero-3-phosphocholine (POPC), and 1-palmitoyl-2-oleoyl-sn-glycero-3-phosphoethanolamine (POPE) and 50% cholesterol (Steraloids, RI). The lipid films were dried as described above but were resuspended in buffer containing HBS pH 7.5, 9 mM DPA pH 11.5, and 3 mM $TbCl_3$ pH 5 for at least half an hour. After rehydration for 30 min, the lipids were subjected to the freeze and thaw cycle and extruded as described above. Next, the vesicles were run through a column packed with Sephadex G-25 Medium resin (GE Healthcare) and equilibrated with HBS pH 7.5 to remove $Tb(DPA)_3^{3-}$ ions not encapsulated by lipids. Fractions were collected in 20-drop aliquots. The concentration of lipids was estimated by measuring scatter at three different wavelengths and using the curves in Figure 2.7.

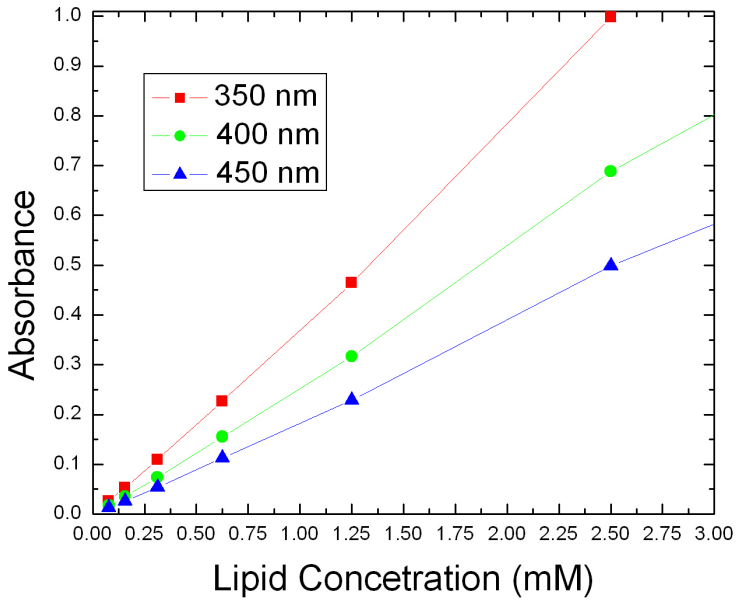

Figure 2.7 Absorbance of liposomes at different wavelengths as a function of lipid concentration.

2.4.6 Analysis of cholesterol binding threshold

In order to establish the cholesterol binding threshold of the labeled PFO, liposomes were prepared using a range of 30-50 mol% cholesterol with a 1:1:1 mol% ratio of SM, POPC, and POPE. Protein at a final concentration of 200 nM was added to buffer containing 50 mM Hepes pH 7.5, 100 mM NaCl, 1mM DTT, and 0.5 mM EDTA, and liposomes of indicated cholesterol concentrations with a final total lipid concentration of 200 μM. Samples were incubated for 20 min at 37 °C in a final volume of 300 μL. PFO binding was determined using the intrinsic Trp emission at 20 ^{o}C before (F_0) and after addition of liposomes (F). Values at each cholesterol mol % are the average of two measurements and the errors bars indicate the range. In the case of the labeled proteins, the increase in fluorescence of the fluorophore was measured. The excitation and emission wavelengths and slits for wtPFO and the labeled derivatives used are described in Table 2.1.

	Excitation wavelength, Slit width	Emission wavelength, Slit width
wtPFO	295 nm, 2 nm	348 nm, 4 nm
NBD	470 nm, 2 nm	530 nm, 4 nm
Acrylodan	380 nm, 2 nm	445 nm, 2 nm

Table 2.1 Excitation and emission wavelengths and respective slit widths for measuring wtPFO and the labeled derivatives.

To examine the lipid composition sensitivity of labeled PFO, liposomes containing 0-50 mol% cholesterol and 1,2-dioleoyl-sn-glycero-3-phosphocholine (DOPC) were prepared and the aforementioned assay was repeated. The resulting cholesterol binding threshold was compared to the binding threshold for the 1:1:1 mol% ratio SM:POPC:POPE-containing liposomes.

2.4.7 Analysis of pore formation

To examine the ability of the labeled derivatives to form pores in cholesterol-containing membranes, the quenching of terbium (Tb^{3+}) in terbium-containing liposomes by EDTA will be examined. Liposomes containing $Tb(DPA)_3^{3-}$ were prepared with a 1:1:1 mol% ratio of SM, POPC, and POPE and 50 mol% cholesterol as described above. Their initial fluorescence was measured in a buffer containing EDTA, which cannot quench fluorescence of Tb^{3+} ions encapsulated in the liposomes. Addition of PFO and subsequent pore formation allows EDTA in the buffer to enter the liposomes, quenching Tb^{3+} fluorescence. Therefore, a resultant decrease in fluorescence indicates that PFO was able to make pores in the liposomes. Fluorescence was measured using an excitation and emission wavelengths of 278 nm and 544 nm, and slit widths of 2 nm and 4 nm respectively. A filter was placed in the emission slit to block emission wavelengths under 300 nm (Barela and Sherry 1976).

2.4.8 Lysis of natural cholesterol-containing membranes by PFO

To measure the hemolytic activity of PFO and the labeled derivatives, protein was serially diluted to the indicated concentrations in a 96-well plate prior to addition of equal volumes of 1% washed sheep red blood cells (RBCs) for a final volume of 250 µL. RBCs were incubated with PFO for 20 minutes at 37 ˚C. The intact RBCs were pelleted by

centrifugation at 3500 x g for 10 min at 4 ˚C. 200 µL of the supernatant was then moved to a new plate where hemoglobin release was measured using absorbance at 540 nm on a plate reader. These values were corrected to 100% hemoglobin release caused by incubation of RBCs with water (causing osmotic shock) and spontaneous hemoglobin release when RBCs were incubated without PFO.

CHAPTER 3

ANALYSIS OF THE TYPE III SECRETION TRANSLOCON

3.1 The role of PopB in PopB/PopD heterocomplex formation

It has been established that *P. aeruginosa* translocons formed when PopB and PopD are added to liposomes consist of 8 PopD monomers and 8 PopB monomers (Romano 2016). When individually added, PopB and PopD form mostly hexamers (Romano 2016). If either translocator is absent, *P. aeruginosa* is unable to translocate toxins into the host cell (Goure 2004), suggesting that only hetero-oligomers are functional for protein translocation. One possible hypothesis for the shift in the stoichiometry of the oligomers is that the translocators form heterodimers and these heterodimers only interact with other heterodimers. In order to investigate the interaction between PopD monomers and PopB/PopD, glutaraldehyde was used as a crosslinker to capture complexes assembled on membranes when PopD was added alone or with an excess of PopB. The interaction was tested by crosslinking and covalently attached subunits were separated in the presence of a strong detergent, Triton X-100.

3.1.1 Addition of PopB assists PopB/PopD heterocomplex formation

In order to efficiently form PopB/PopD complexes on membranes, purified PopD and PopB were added to liposomes at acidic pH (pH 4.3) as described previously (Romano 2016). Previous data has shown that an excess of PopB is needed to force PopD into heterocomplexes and minimize formation of homo-complexes. The reconstitution reaction contained a 7:1 molar ratio of PopB to PopD with a total protein to lipid ratio of

1:6000 (Romano et al 2016). After inserting into the membrane, assembled complexes were crosslinked with glutaraldehyde and analyzed via western blot.

When PopD alone was incubated with liposomes, high-order oligomers that correspond to PopD dimers (62.6 kDa), trimers (93.9 kDa), and pentamers (156.5 kDa) were observed (Figure 3.1). However, with the addition of PopB, there is a clear shift in bands, which correlate to PopB and PopD complexes (right lane, Figure 3.1). This indicates that the addition of PopB redirects the oligomerization state of PopD from homo-oligomers to hetero-oligomers.

Previous results suggested that PopD homo-oligomers were stable to Triton X-100, but not the hetero-oligomers (for example, the inability to purify heterocomplexes, unpublished results). In order to understand the stability of this interaction, PopD alone and PopB and PopD were allowed to form oligomers and then incubated with Triton X-100 to solubilize the membrane. Association of the complexes was tested using glutaraldehyde crosslinking. The complexes that remained associated were then captured by crosslinking, while dissociated complexes were not. Crosslinking experiments corroborated that PopD alone is stable to solubilization with Triton X-100 but PopB and PopD are not able to form stable complexes in the presence of Triton X-100 (Figure 3.2). The addition of Triton X-100 is able to disassociate PopB/PopD complexes as shown by the lack of bands at molecular weights above the PopD monomer (31 kDa).

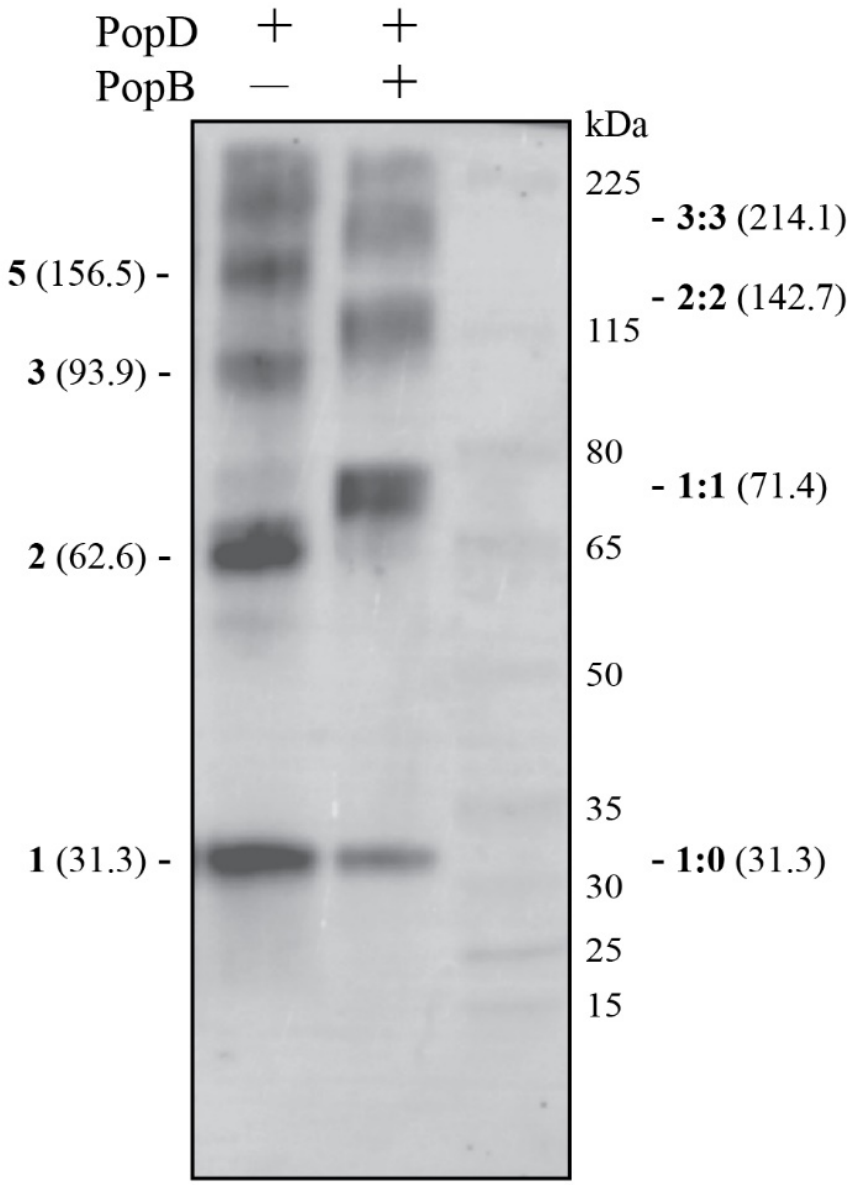

Figure 3.1 Capturing complexes with glutaraldehyde glutaraldehyde cross-linking of PopD homo-oligomers and PopB and PopD hetero-oligomers formed on liposomes. PopD alone or premixed with an excess of PopB were incubated with liposomes in buffer B for 20 min with a protein:lipid ratio of 1:5000. Proteoliposomes were pelleted and subjected to immunoblotting using an anti-PopD antibody. Expected molecular masses for PopD *n*-mers (*left*) and PopD:PopB *n*-mers (*right*) were estimated using the molecular mass for PopD (31.3 kDa) and PopB (40.1 kDa) monomers. Published in Tang et al 2018.

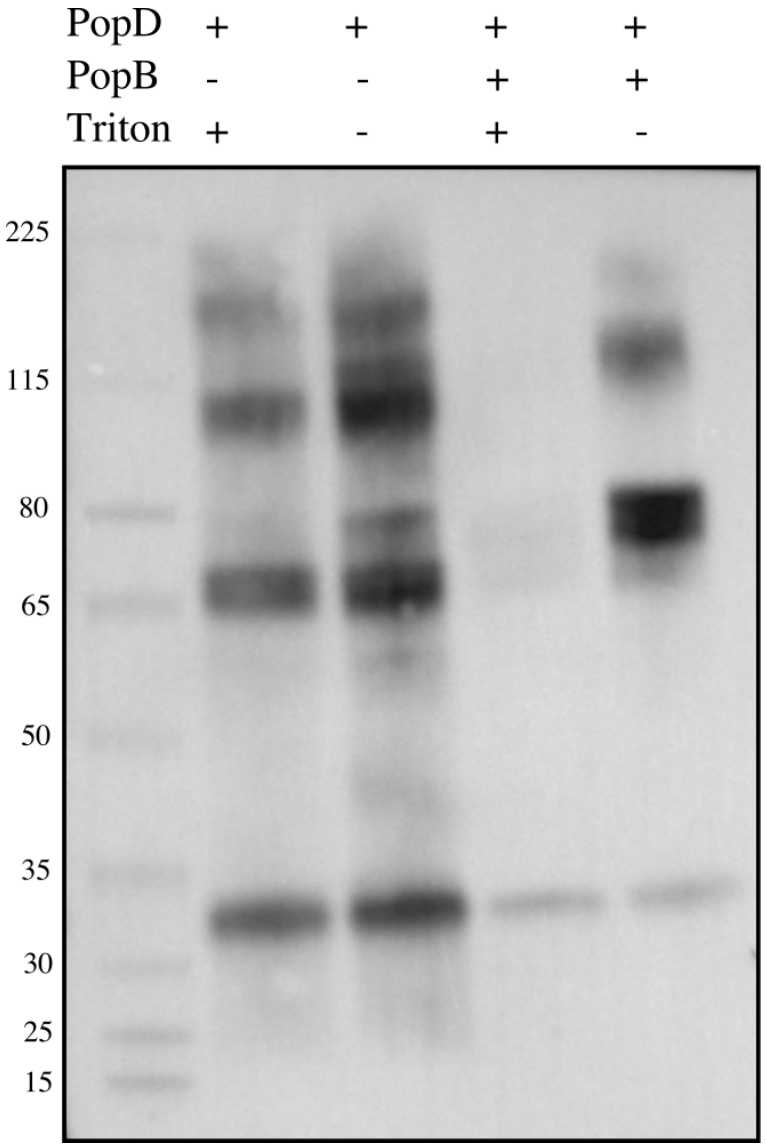

Figure 3.2 PopD homo oligomers are stable to Triton X-100 solubilization while PopB/PopD heterocomplexes are not. PopB/PopD or PopD alone was added to liposomes at pH 4.3 before the addition of Triton X-100. The resulting complexes were crosslinked with glutaraldehyde to capture oligomers stable to Triton X-100 before TCA precipitating and western blotting against PopD.

3.2 ybbR tag inserted into PopD after residues 40 and 208 does not impede the formation of a functional translocon

It has been established that the conformation of PopD is influenced by the presence of the other translocator, PopB (Tang et al 2018). Additionally, it is known that in vivo, the N terminal region of PopD is exposed to host cell cytosol (Tang et al 2018). By using strategically placed GSK tags that are phosphorylated only when exposed to the host cell, Tang was able to explore the topological arrangement of PopD in functional translocons (Tang 2018). Phosphorylation experiment results showed that PopD derivatives with GSK tags placed after residue 40, 29, 157, 178, and 237 were phosphorylated by the host cell, indicating that these residues are located on the inside of the host cell membrane (Tang 2018). Unfortunately, the GSK tag does not provide any information on the segments of the translocators that remain outside the cell.

In order to further understand the topology of the translocator, PopD, we have created three different strains with a ybbR tag inserted after different residues in PopD. The ybbR tag, an 11-residue peptide (DSLEFIASKLA), can be labeled by Sfp phosphoopantetheinyl transferase (Sfp) with small molecule-CoA conjugates (Yin et al 2005). Sfp transfers the 4'-phosphopantetheinyl group of CoA onto the serine residue in the ybbR peptide and can also transfer small molecules that are attached to CoA, such as the fluorophore Alexa488.

By infecting HeLa cells with these strains and subsequently labeling inserted PopD with Alexa488-CoA, it will be possible to determine if the residues are exposed to the extracellular media or not. It is also necessary to confirm the functionality of modified PopD because without proper secretion and insertion in the membrane, it will be impossible to use as a target for Alexa488-CoA labeling. In other words, if the

modified PopD cannot form a functional translocon in the host cell membrane, the translocon may not be inserted properly and any structural information we obtain would be inaccurate.

We chose to insert the ybbR tag after residue Q40, I83, and S208. While it has already been shown that residue V29, Q40, K157, D178, and E237 located in the N terminus of PopD, is exposed to the host cell cytosol, the location of the two other residues is unknown but predicted to be exposed to the extracellular media (Tang 2018). Additionally, it has been shown that a GSK tag insertion after residue S208 does not impede translocon formation (Tang 2018). However, the effect of any tag insertion after residue I83 has yet to be characterized.

3.2.1 ybbR-tagged PopD strains secrete PopB and PopD

In order to expand upon our knowledge of the topology of PopD inserted in HeLa cell membranes, we created three different plasmids with a ybbR tag inserted after residue Q40, I83, and S208 in PopD. The Q40 substitution is predicted to be exposed to the host cell cytosol, so is therefore the negative control for the labeling assay. The I83 and S208 residue are both predicted to be exposed to the extracellular media. The plasmids were then transformed into *P. aeruginosa* PAK ΔpopD strains. As a negative control for PopD secretion, *P. aeruginosa* PAK ΔpopD was transformed with an empty plasmid (pUCP18) while our positive control was *P. aeruginosa* PAK ΔpopD complemented with a plasmid containing PopD WT.

In order to test that the ybbR-tag strains can secrete both translocators at levels comparable to wild-type, secretion was induced by inducing low calcium conditions. It has been shown that low calcium can cause T3S upregulation and secretion (Goure 2004, Vallis 1999). Culture media containing the secreted protein was separated from bacteria

and precipitated by TCA. Samples were analyzed by western blotting against PopB and PopD antibodies (Figure 3.3). Blots were subsequently analyzed by comparing band intensity between samples using ImageJ (Figure 3.4). The strains complemented with ybbR-tagged PopD secreted levels comparable to the one observed for PopD WT.

3.2.2 PopD with a ybbR tag after residue 40 and 208 but not 83 can form a functional translocon on HeLa cell membranes

To test if the ybbR tag insertion affects the function of PopD to infect mammalian cells, we incubated HeLa cells with the indicated strain at a bacteria:cell ratio of 10:1 (multiplicity of infection, or MOI, 10) and screened for cell rounding, an indicator of HeLa cell distress (Fig. 3.5). After a 2.5 hour-long infection, cell rounding was observed in the cells infected with PAK strains containing PopD WT and the strains with the ybbR tags inserted after residue 40 and 208 (Figure 3.5). The strain with PopD 40-ybbR caused cell rounding at rate comparable to PopD WT, causing HeLa cells to detach from the plates after 2.5 hours of infection. While at 2.5 hours the PopD 208-ybbR had only caused HeLa cells to round and not detach, extending the infection caused the cells to all round and detach (data not shown). In contrast to the other two ybbR-tagged strains, the PopD 83-ybbR strain exhibited no cell rounding (Figure 3.5). In fact, there was no noticeable difference between HeLa cells infected with PAK ΔpopD:pUCP18 or PAK ΔpopD::popD 83-ybbR, even at longer time points. These results demonstrate that the addition of the ybbR tag after residue 40 and 208 of PopD does not impede the formation of a functional translocon, but the insertion after residue 83 does.

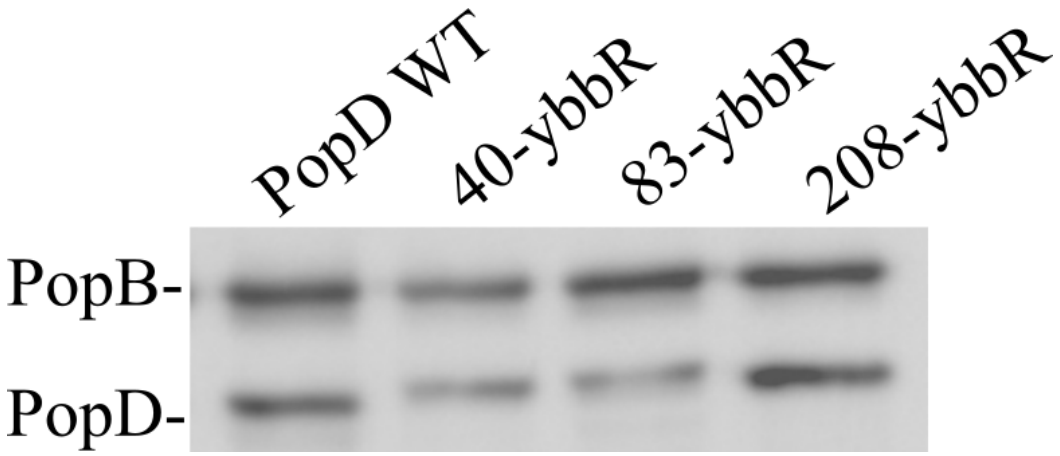

Figure 3.3 Secretion of T3S translocators in strains containing modified PopD. *P. aeruginosa* cultures containing the indicated PopD were induced to secrete in low calcium conditions. Protein was collected and precipitated by TCA and analyzed using SDS-PAGE and western blot. Antibodies used were a mixture of polyclonal anti-PopB and anti-PopD antibodies.

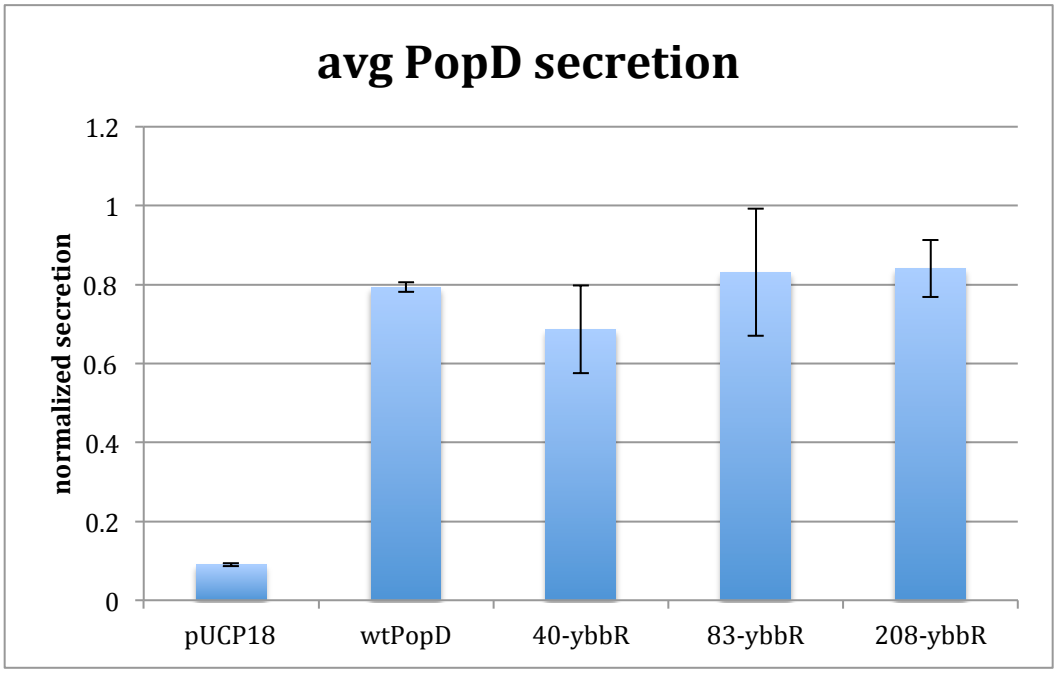

Figure 3.4 Graphical representation of PopD secretion, normalized to PopB secretion. Band intensity was quantified using ImageJ. PopD band intensity was normalized to PopB band intensity. Bars represent average of two experiments and error bars show the range.

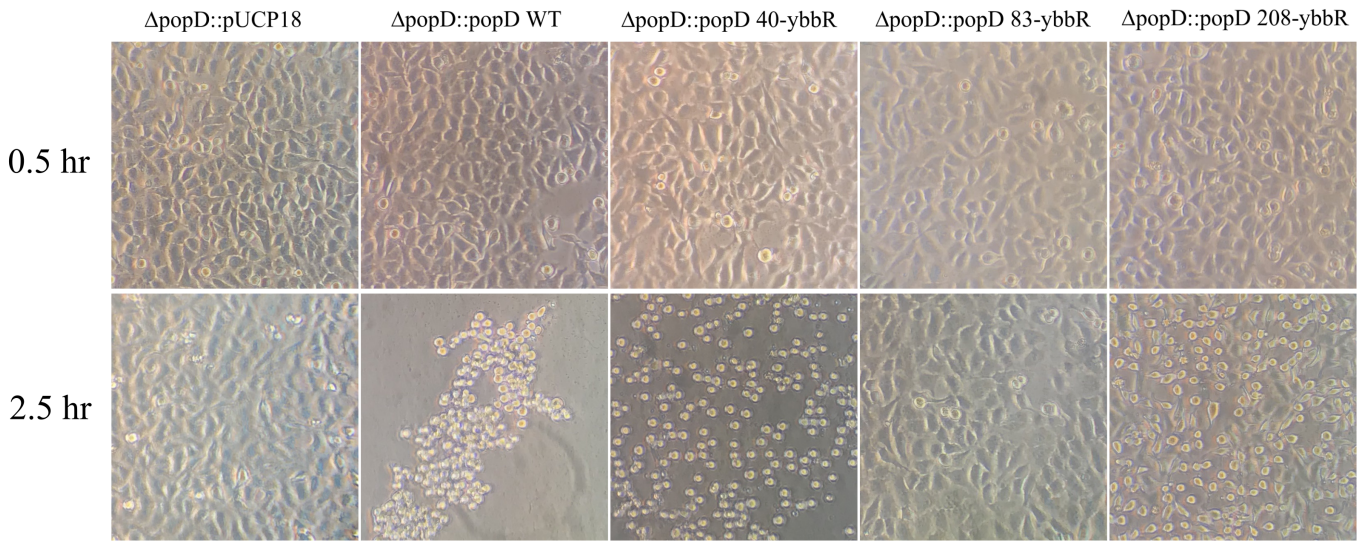

Figure 3.5 PAK ΔpopD strains complemented with ybbR-tagged PopD cause cell rounding in HeLa cells. HeLa cells were infected with *P. aeruginosa* PAK complemented with the indicated plasmid. Representative images at 30 min of infection (top row) and 2.5 hours of infection (bottom row) are shown. Multiplicity of infection (MOI) 10.

3.2.3 PopB and PopD bind to HeLa cell membranes

In addition to measuring the HeLa cell rounding, we also compared the amount of PopB and PopD inserted on HeLa cell membranes after infection. Following the protocol published by Tang et al (2018), HeLa cells were infected with an effector-less ΔpopD PAK strain complemented by the empty pUCP18 plasmid, a plasmid containing PopD WT, or the tagged PopD plasmids. Following infection, the bacteria-infected cell membrane was isolated and membrane bound translocators were analyzed via western blot (Figure 3.6). Both translocators, PopB and PopD, were detected bound to HeLa cell membranes in all of the ybbR-tagged strains.

3.2.4 GST-ybbR can be labeled in the presence of HeLa cells

In order to confirm that the labeling reaction is able to take place in the presence of HeLa cells, ybbR-tagged glutathione-S-transferase (GST-ybbR) was added to a flask containing HeLa cells. A total of 2 mL of the labeling reaction containing Sfp and Alexa488 conjugated CoA was added to the flask and allowed to incubate for 2 hours at room temperature. The media containing labeled GST-ybbR was removed and scanned with a GE Typhoon phosphorimager (Figure 3.7). The presence of the band at approximately 26 kDa indicates that GST was successfully labeled in the presence of HeLa cells. In other words, the labeling reaction takes place under our experimental conditions.

3.2.5 PopD 40-ybbR can be secreted into the media and labeled with Alexa488

With the necessary characterization in place, we were able to proceed and attempt to label ybbR-tagged PopD in vivo by infecting HeLa cells with ybbR-tagged PopD and adding the labeling reaction after removing the bacteria. Unfortunately, this yielded no

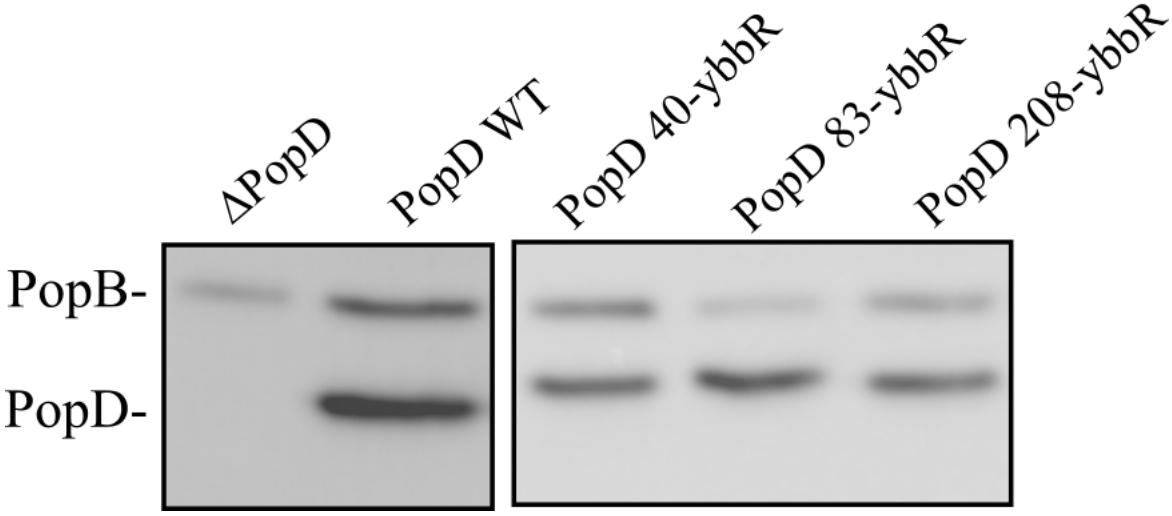

Figure 3.6 Binding of translocators to HeLa cell membranes. HeLa cells were infected with an effector less *P. aeruginosa* PAK strain (PAK ΔESTY ΔD) complemented with the indicated plasmid at an MOI of 30. The membrane fractions were isolated and chloroform/methanol precipitated before being analyzed via western blot. 20 ng of total protein was loaded per lane.

Figure 3.7 GST-ybbR is successfully labeled with Alexa488 in the presence of HeLa cells. GST-ybbR was added to a flask containing HeLa cells, Sfp, and Alexa488-CoA. The solution containing GST-ybbR was removed and chloroform/methanol precipitated and 0.2 μg of protein was loaded onto a 12.5% acrylamide SDS-PAGE gel. Gel was imaged with a GE Typhoon phosphorimager.

visible bands when imaging the gel, which led us to see if ybbR-tagged PopD could be secreted by *P. aeruginosa* and labeled without being inserted in the membrane.

To see if the ybbR-tagged PopD constructs could be secreted by *P. aeruginosa* and subsequently be labeled by Alexa-CoA, we induced secretion by creating low-calcium conditions (as described above). After pelleting the bacteria, Sfp and Alexa488-CoA was added to the culture containing secreted proteins to label ybbR tagged PopD. Out of all of the ybbR-tagged PopD constructs, PopD 40-ybbR was the only one that was successfully labeled with Alexa488 (Fig. 3.8).

3.3 Discussion

In order to understand the interaction between PopB and PopD on model membranes, glutaraldehyde crosslinking was used to study the complexes assembled on liposomes. We found that the addition of PopB to PopD redirects the formation of PopD homocomplexes to PopB/PopD heterocomplexes when incubated on liposomes, suggesting the early formation of heterodimers. This is supported by the finding that PopD oligomers do remain associated in the presence of Triton X-100, while PopD-PopB oligomer do not.

To study the regions of the translocators exposed to the extracellular media, we created three different strains with ybbR tags inserted after either residue 40, 83, and 208 in PopD. We then proceeded to characterize the functionality of the ybbR-tagged PopD by assessing translocator secretion, HeLa cell cytotoxicity, and HeLa cell membrane binding.

All of the ybbR-tagged PopD constructs were found to secrete both translocators at comparable levels to PopD WT (Figure 3.3 and 3.4). In order to quantify PopD secretion and control for sample loading, PopD band intensity was normalized to PopB

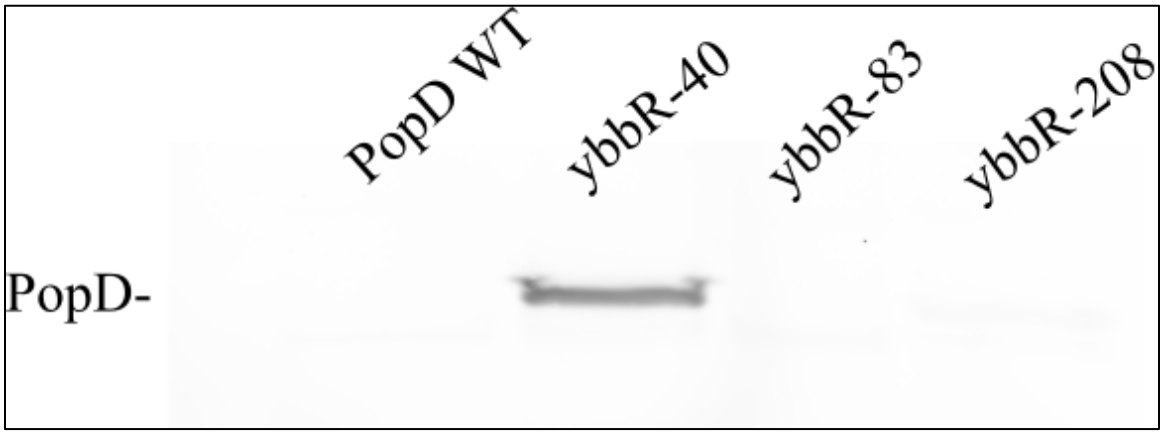

Figure 3.8 PopD 40-ybbR can be labeled by Alexa488-CoA when secreted to the media. *P. aeruginosa* strains containing the indicated plasmids were induced to secrete under low calcium conditions. The secreted proteins were isolated and incubated with Sfp and Alexa488-CoA to label the ybbR tag. Samples were TCA precipitated and loaded onto a 12.5% acrylamide gel before being imaged with a GE Typhoon phosphorimager.

intensity. Because PopB was not modified in any of the strains used, the secretion of PopB should have been the same in every strain tested.

While all of the ybbR-tagged strains were able to secrete both translocators, there were differences in HeLa cell cytoxicity. We found that only the strains containing PopD40-ybbR and PopD208-ybbR exhibited cell rounding comparable to ΔpopD::PopD WT (Figure 3.5). These results were expected based on the successful insertion of a GSK tag after residues 40 and 208 used by Tang et al (2018). However, PopD83-ybbR appeared to cause no cell rounding compared to PopD WT, even when infection times were extended. While PopD83-ybbR is secreted, the lack of cell rounding indicates that PopD83-ybbR may not adopt the correct orientation or insert into the HeLa cell membrane.

We were able to confirm that all three PopD derivatives were able to associate with HeLa cell membranes (Figure 3.6). By infecting HeLa cells with an effector less *P. aeruginosa* PAK ΔESTY ΔpopD strain complemented with a plasmid containing no PopD, PopD WT, or ybbR-tagged PopD, and subsequently isolating the membrane-bound proteins, we were able to confirm the ability of *P. aeruginosa* to successfully inject a translocon containing ybbR-tagged PopD that can bind to the cell membrane.

Lastly, we were able to show that the labeling reaction was able to take place in the presence of HeLa cells (Figure 3.7). Further, by controlling the amount of substrate to be labeled we now have a benchmark for the amount of substrate necessary to produce a visible band in the gel.

While these positive results indicated that we are able to move forward and attempt to label the ybbR tag in vivo with Alexa488-CoA using Sfp phosphoopantetheinyl transferase, such attempts were not successful. However, we were able to confirm that PopD 40-ybbR can be labeled when it is secreted to the media (Figure 3.8). This corroborates previous studies, which have shown that residue Q40 in PopD is exposed to the cytosol when inserted in HeLa cell membranes (Tang et al 2018). However, when inserted into the membrane, we expect that the ybbR tag inserted after residue 40 will not be labeled by Alexa488-CoA, and it will serve as a negative control for the labeling reaction. However, it is unclear where the other two locations with a ybbR tag (residue 83 and 208) are located when a functional PopB/PopD translocon is assembled in HeLa cell membranes. Because the strains containing PopD83-ybbR do not form functional translocons, this construct will not be used in the analysis.

3.4 Materials and methods

3.4.1 Purification of PopB and PopD

As described previously in Romano et al 2011.

3.4.2 Liposome preparation

As described in 2.4.4. Briefly, all lipids except cholesterol (Steraloids) were purchased from Avanti Polar Lipids and are stored as solutions dissolved in chloroform. Lipids were mixed in the following ratios: 65 mol% 1-palmitoyl-2-oleoyl-sn-glycero-3-phosphocholine (POPC), 15 mol% 1-palmitoyl-2-oleoyl-sn-glycero-3-phospho-L-serine (POPS), and 20 mol% cholesterol (Steraloids, RI) to a final concentration of 30 mM.

3.4.3 Crosslinking

Purified PopD alone or a mixture of PopD and PopB in 6 M Urea, and NaCl, glycine, and Tris (20mM, pH 8) were diluted and incubated with liposomes in a total of 200 µl 20 mM sodium acetate, pH 4 for 20 min at room temperature (20-23˚C). Final

concentrations were 800 nM total protein and 4.8 mM total lipids. The pH of the reaction was raised to neutral (pH 7) titration with buffer containing 1 M Hepes pH 8.0 (~30 µl). If detergent was used, prior to crosslinking, Triton X-100 (6.2 µM final concentration) was added to reaction for 5 min. A 1% glutaraldehyde solution (Sigma) was freshly prepared and added to the reconstitution reaction with a final concentration of 0.01% glutaraldehyde. This reaction was incubated for 2 min at room temperature and stopped with the addition of 1 M Tris, pH 8.0 to a final concentration of 150 mM and allowed to incubate for 20 min at room temperature. The sample was then TCA precipitated and resuspended in 20µL loading buffer (4% 2-mercaptoethanol, 50 mM Tris pH 6.8, 10% v/v glycerol, 2% w/v SDS, 5 mM EDTA, 0.02% bromophenol blue). This sample was run on a 4-12% ExpressPlus PAGE gels (GenScript), and probed for PopD by immunoblotting using anti-PopD (diluted 1: 4000) polyclonal antibodies.

3.4.4 Western blot

As described previously in Tang et al 2018. In the case of crosslinking, protein was separated on a 4-12% ExpressPlus PAGE gels. Others were run on 12.5% acrylamide SDS-PAGE gels.

3.4.5 HeLa cell rounding

HeLa cells were seeded at confluency on 6-well plates (Falcon) prior to the addition of indicated *P. aeruginosa* strains at an MOI of 10. HeLa cells were monitored every half hour and screened for cell rounding.

3.4.6 Secretion assay

Overnight (ON) cultures were set up in autoclaved glass test tubes with a total volume of 4 mL with 300 µg/mL carbenicillin and incubated at 37 ˚C at 225 rpm. The following morning, they were diluted to obtain 3 mL of OD600 0.1-0.15 with fresh LB

(no antibiotics) and grown for an additional 2 hrs shaking at 37˚C. Secretion of T3S substrates was induced with EGTA (5 mM final concentration) and $MgCl_2$ (20 mM final concentration). Bacteria were allowed to grow for additional 1.5 hrs under the low calcium condition. Aliquots of 1 ml of bacterial culture were pelleted at 16,000 x g for 15 min, and were normalized by measuring OD600 using rest of the culture and were diluted further with LB if needed. Quantification of secreted proteins will be normalized to same number of bacteria calculated using OD600 of 1 = 2 x 108 cells. The cleared supernatant containing secreted proteins was collected and precipitated by TCA. Samples were analyzed by immunoblotting using anti-PopB (diluted 1:200,000) and anti-PopD (diluted 1:4,000) antibodies. The secreted amount of PopB and PopD were quantified using ImageJ. In the case of Alexa488-CoA labeling, the labeling reaction was added directly to the supernatant to a final concentration of 100 mM $MgCl_2$, 50 mM Hepes pH 7.5, 1 μM Sfp, and 5 μM Alexa488-CoA and allowed to incubate at 20-23 ˚C for one hour. Samples were TCA precipitated and analyzed by running on an SDS-PAGE prior to imaging with a GE Typhoon phosphorimager.

3.4.7 HeLa cell binding

As described in Tang et al 2018.

3.4.8 GST-ybbR labeling in presence of HeLa cells

HeLa cells were cultured in T25 flasks (Corning) and the media (DMEM, Hyclone) was removed prior to washing 3x with DPBS (Hyclone). To the flask, 2 mL of a labeling reaction was added containing a final concentration of 100 mM $MgCl_2$, 50 mM Hepes pH 7.5, 1 μM Sfp, 5 μM Alexa488-CoA and 5 μM GST-ybbR. The GST-ybbR, Sfp, and Alexa488-CoA were given by Fabian Romano.

CHAPTER 4

CONCLUSION

4.1 Summary of the effect of a fluorophore-modified Cys on PFO binding and pore formation

To modify the Cys459 residue, we used two thiol-reactive fluorescent labels: IANBD (NBD) and acrylodan. In addition to the change in binding threshold that a Cys modification would produce, the presence of environmentally sensitive fluorophores allowed us to directly monitor the interaction of the undecapeptide with the membrane. By using a series of assays that measure the cholesterol-dependence of these PFO derivatives on model membranes, its ability to form pores, and their hemolytic activity on sheep red blood cells, we characterized how these modifications alter the cholesterol recognition properties of wild type PFO.

In comparison to wtPFO, we found that the modification to the Cys residue with acrylodan or NBD did not have a significant impact on the cholesterol binding threshold. However, the labeled derivatives were not as efficient as wtPFO in forming pores in both naturally cholesterol-containing membranes and liposomes. These results tell us that while the modification on D4 did not significantly affect cholesterol recognition, there was an impact on the ability to insert the β hairpins to form a pore. These results suggest that Cys459 may be involved in the allosteric conformational changes that trigger oligomerization and insertion of the β-barrel.

4.1.1 Future directions

It was previously demonstrated that using a thiol-blocking agent on the conserved Cys in wtPFO can block hemolytic activity, suggesting that this Cys residue is important

for binding and ultimately pore formation (Iwamoto et al 1987). However, the mechanism for this inhibition was unclear. Based on our results, the addition of a hydrophobic thiol-reactive probe is not enough to inactivate the toxin. Therefore, it would be interesting to observe effect of other Cys modifications on cholesterol binding and pore formation. For example, introducing molecules with either a positive or a negative charge and measuring cholesterol binding would give insights on the interaction between PFO and the membrane.

4.2 Summary of T3S system translocon analysis

We have shown that PopB and PopD interact on membranes to form heterocomplexes. Additionally, we have begun the characterization of a *P. aeruginosa* PopD knockout strain complemented with ybbR-tagged PopD in the hopes of labeling the ybbR tag in vivo. A ybbR tag was inserted after three different residues in PopD, residue Q40, I83, and S208, and the plasmids containing these ybbR-tagged PopD constructs were transformed into *P. aeruginosa* PAK PopD-knockout strains. These strains were characterized by their HeLa cell cytotoxicity through cell rounding, ability to secrete both translocators, and ability to bind to HeLa cell membranes. Additionally, we were able to show that the labeling reaction is able to proceed in the presence of HeLa cells by labeling GST-ybbR in the presence of HeLa cells. However, we were unable to successfully label any of the tags in vivo.

4.2.1 Future directions

Based on our positive labeling results, in order to successfully label PopD in vivo and analyze the position of the residues, the conditions for labeling will have to be optimized. While we have shown that the translocators in PopD40-ybbR and PopD208-ybbR are functional and able to bind to HeLa cell membranes, in vivo labeling was not

successful. This may be because there is not enough substrate present for Sfp to label, in which case the experiment would need to be scaled up or a more sensitive method of screening for labeling will need to be explored. By using a Typhoon phosphorimager, we are able to detect as low as 0.2 μg of labeled protein. If our in vivo labeling is unable to produce 0.2 μg of labeled PopD, it will be necessary to explore other more sensitive methods of fluorophore detection, such as fluorescent microscopy. Additionally, increasing the sample would be costly; therefore, a more sensitive method of fluorophore detection would be more practical.

However, there are other labeling methods that would avoid this issue. Because PopD does not have a native cysteine, introducing a Cys substitution would allow us to perform PEGylation assays. By using PEG-maleimide, a reagent that reacts with the sulfhydryl group of the cysteine, we would be able to observe a shift in the molecular weight of PopD if the Cys residue is exposed or not. This assay would also avoid the need for increasing sample size because the antibodies we have are already sensitive enough to detect the amount of PopD that is bound to HeLa cell membranes. Additionally, because our PopD83-ybbR construct was not able to form a functional translocon on HeLa cell membranes, in order to understand the position of this residue it will be necessary to pursue other types of labeling reactions. It is possible that the ybbR tag interferes with proper insertion and therefore a less intrusive modification might be more successful. For these reason, a Cys substitution and PEGylation assay would be a practical method to explore the topology of PopD.

APPENDIX

SOME CHARACTERIZATION OF THE INACTIVE PFO TOXIN, pPFO

A.1 Labeling of of pPFO with Alexa488 does not affect the cholesterol threshold

Due to the lytic properties exhibited by full-length PFO, there has been a need for non-lytic cholesterol probes. One such probe was generated by Johnson et al that contained four amino acid substitutions: C459A, E167C, Y181A, and F318A, generating a so-called parental PFO, or pPFO (Johnson et al 2017). The Cys substitutions allow for labeling on a residue that does not interact with the membrane and the Y181A and F318A substitutions render the toxin inactive (Johnson et al 2017). Here, the effect of labeling E167C with Alexa488 on the cholesterol binding threshold was measured.

In order to see if Alexa labeling interfered with the cholesterol binding threshold of pPFO, the cholesterol binding curve of Alexa488-labeled pPFO was compared to the curve for unlabeled pPFO. Alexa488-labeled pPFO or pPFO were incubated with liposomes containing 30-42 mol% cholesterol and the resultant increase in Trp fluorescence was measured. There was no difference in the cholesterol binding threshold between Alexa488-labeled pPFO and unlabeled pPFO (A0.1).

A.2 Cholesterol-dependent binding isotherms for pPFO

In order to observe the effect of high concentrations of pPFO on the typical sigmoidal cholesterol binding curve, different concentrations of pPFO were incubated

with liposomes. Following incubation, the resultant increase in Trp fluorescence was compared to the initial fluorescence. We found that at high concentrations of protein, the

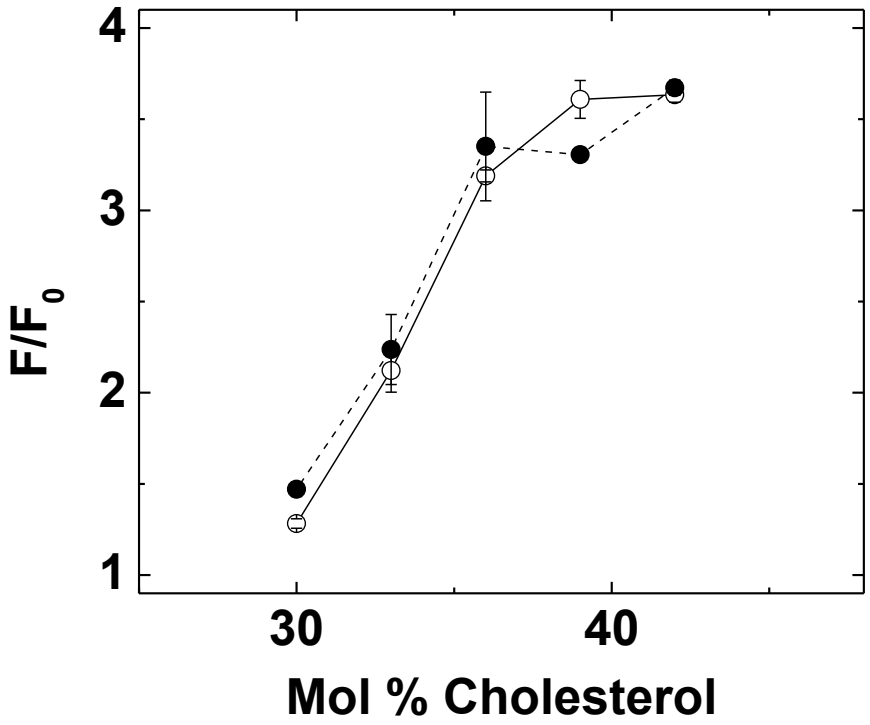

Figure A.1 Labeling of pPFO with Alexa488 does not affect the cholesterol threshold. pPFO (open circles) and $pPFO^{Alexa488}$ (filled circles) were added to a final concentration of 0.2 μM, and incubated with liposomes of varying cholesterol concentrations and a constant 1:1:1 molar ratio of POPC, POPE, and SM (final total lipid concentration of 0.2 mM). PFO binding was determined using the intrinsic Trp emission before (F_0) and after addition of liposomes (F) at 20 ^{o}C. Values at each cholesterol mol % are the average of two measurements and the errors bars indicate the range. Published in Johnson et al 2017.

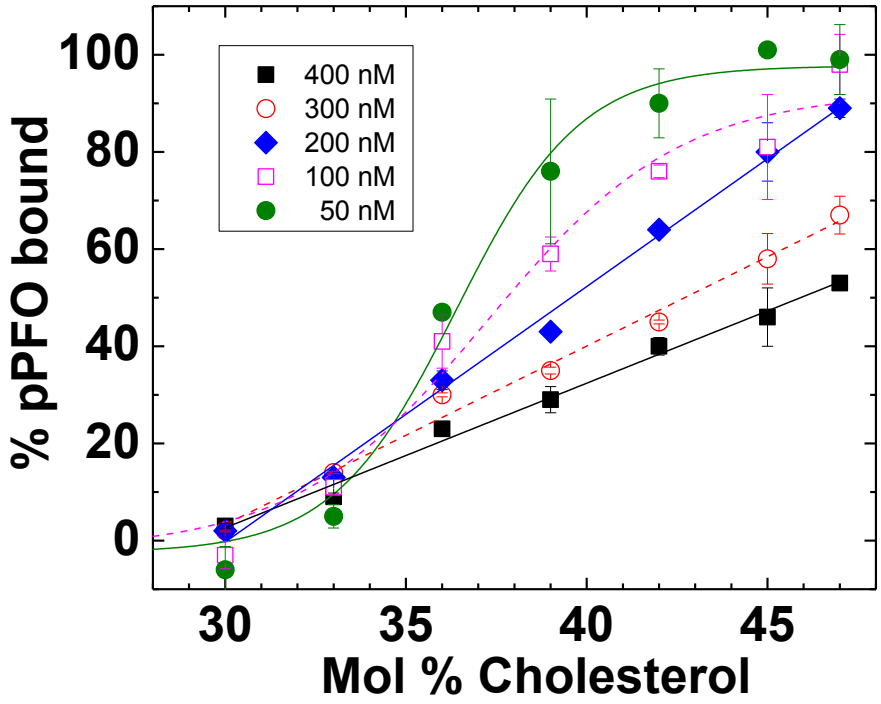

Figure A.2 Cholesterol-dependent binding isotherms for pPFO. pPFO at the indicated final concentration was incubated in 50 mM buffer Hepes pH 7.5, 100 mM NaCl, 1mM DTT, and 0.5 mM EDTA with liposomes of varying cholesterol concentrations and a constant 1:1:1 molar ratio of POPC, POPE, and SM (final total lipid concentration of 50 μM). Samples were incubated for 20 min at 37 °C in a final volume of 300 μL. PFO binding was determined using the intrinsic Trp emission at 20 ^{o}C before (F_0) and after addition of liposomes (F) as described in methods. Values at each cholesterol mol % are the average of two measurements and the errors bars indicate the range. Published in Johnson et al 2017.

typical sigmoidal curve becomes linear (Fig. A0.2). These results corroborated the findings in Johnson et al which suggested that high concentrations of pPFO saturate the membrane of RAW264.7 cells (Johnson et al 2017).

REFERENCES

Anantharajah, A., Mingeot-Leclercq, M. P., and Van Bambeke, F. (2016) Targeting the Type Three Secretion System in Pseudomonas aeruginosa. *Trends Pharmacol Sci* **37**, 734-749

Barela, T. D. & Sherry, A. D. (1976) A simple, one-step fluorometric method for determination of nanomolar concentrations of terbium. *Anal. Biochem.* **71**, 351-357

Costa, T. R. D. *et al.* (2015) Secretion systems in Gram- negative bacteria: structural and mechanistic insights. *Nat. Rev. Microbiol.* **13**, 343–359.

Courtney, K. C., Fung, K. Y., Maxfield, F. R., Farin, G. D., Zha, X. (2018) Comment on 'Orthogonal lipid sensors identify transbilayer asymmetry of plasma membrane cholesterol. *Elife.* **7**.

Deng, W., Marshall, N. C., Rowland, J. L., McCoy, J. M., Worrall, L. J., Santos, A. S., Strynadka, N. C. J., and Finlay, B. B. (2017) Assembly, struc- ture, function and regulation of type III secretion systems. *Nat. Rev. Mi- crob.* **15,** 323–337

De Smet, J., Hendrix, H., Blasdel, B. G., Danis-Wlodarczyk, K., and Lavigne, R. (2017) Pseudomonas predators: understanding and exploiting phage-host interactions. *Nat Rev Microbiol* **15**, 517-530

Dortet, L., Lombardi, C., Cretin, F., Dessen, A., Filloux, A. (2018)Pore- forming activity of the *Pseudomonas aeruginosa* type III secretion system translocon alters the host epigenome. *Nat. Microb.* **3,** 378 –386

Farrand, A.J.; LaChapelle, S.; Hotze, E.M.; Johnson, A.E.; Tweten, R.K. (2010) Only two amino acids are essential for cytolytic toxin recognition of cholesterol at the membrane surface. *Proc. Natl. Acad. Sci. USA*, *107*, 4341–4346.

Flanagan, J. J., Tweten, R. K., Johnson, A. E. & Heuck, A. P. (2009) Cholesterol exposure at the membrane surface is necessary and sufficient to trigger perfringolysin O binding. *Biochemistry* 48, 3977–3987.

Folkesson, A., Jelsbak, L., Yang, L., Johansen, H. K., Ciofu, O., Hoiby, N., and Molin, S. (2012) Adaptation of Pseudomonas aeruginosa to the cystic fibrosis airway: an evolutionary perspective. *Nat Rev Microbiol* **10**, 841-851

Gay A, Rye D, Radhakrishnan A. (2015) Switch-like Responses of Two Cholesterol Sensors Do Not Require Protein Oligomerization in Membranes. *Biophysical Journal*. 108(6):1459-1469.

Gimpl, G. & Gehrig-Burger, K. (2011) Probes for studying cholesterol binding and cell biology. *Steroids* 76, 216–231.

Gellatly, S. L., and Hancock, R. E. (2013) Pseudomonas aeruginosa: new insights into pathogenesis and host defenses. *Pathog Dis* **67**, 159-173

Goure, J., Pastor, A., Faudry, E., Chabert, J., Dessen, A., and Attree, I. (2004) The V antigen of Pseudomonas aeruginosa is required for assembly of the functional PopB/PopD translocation pore in host cell membranes. *Infect Immun* **72**, 4741-4750

Hauser, A. R., Cobb, E., Bodi, M., Mariscal, D., Valles, J., Engel, J. N., and Rello, J. (2002) Type III protein secretion is associated with poor clinical outcomes in patients with ventilator-associated pneumonia caused by Pseudomonas aeruginosa. *Crit Care Med* **30**, 521-528

Heuck A.P., Hotze E.M., Tweten R.K., Johnson A.E. (2000) Mechanism of membrane insertion of a multimeric β-barrel protein: Perfringolysin O creates a pore using ordered and coupled conformational changes. *Mol. Cell* 6, 1233–1242.

Heuck A.P., Moe P.C., Johnson, B.B. (2010). The cholesterol-dependent cytolysins family of Gram-positive bacterial toxins. *Subcellular Biochemistry* **51**:551-77.

Heuck, A. P., Savva, C. G., Holzenburg, A., Johnson, A. E. (2007) Conformational changes that effect oligomerization and initiate pore formation are triggered throughout Perfringolysin O upon binding to cholesterol. *J. Biol Chem*. 282, 22629-22637.

Hoiby, N., Ciofu, O., and Bjarnsholt, T. (2010) Pseudomonas aeruginosa biofilms in cystic fibrosis. *Future Microbiol* **5**, 1663-1674

Hotze, E. M., A.P. Heuck, D.M. Czajkowsky, Z. Shao, Johnson, A.E., Tweten, R.K. (2002) Monomer-monomer interactions drive the prepore to pore conversion of a β-barrel-forming cholesterol-dependent cytolysin. *J. Biol. Chem*., 277, 11597-11605.

Hueck, C.J. (1998) Type III protein secretion systems in bacterial pathogens of animals and 23 plants. *Microbiology And Molecular Biology Reviews* **62**(2): 379-433.

Hu, B., Lara-Tejero, M., Kong, Q., Galan, J. E., and Liu, J. (2017) In Situ Molecular Architecture of the Salmonella Type III Secretion Machine. *Cell* **168**, 1065-1074

Hu, B., Morado, D. R., Margolin, W., Rohde, J. R., Arizmendi, O., Picking, W. L., Picking, W. D., and Liu, J. (2015) Visualization of the type III secretion sorting platform of Shigella flexneri. *Proc Natl Acad Sci U S A* **112**, 1047-1052

Iwamoto M., Ohno-Iwashita Y., Ando, S. (1987) Role of the essential thiol group in the thiol-activated cytolysin from *Clostridium perfringens*. *Eur. J. Biochem*. **167**, 425-430.

Johnson, B. B. (2014) Engineering Probes to Detect Cholesterol Accessibility on Membranes Using Perfringolysin O. *Doctoral Dissertations*. 97.

Johnson, B.B., Breña, M., Anguita, J., Heuck, A.P. (2017) Mechanistic insights into the cholesterol-dependent binding of perfringolysin O-based probes and cell membranes. *Sci. Rep*. **7**, 13793.

Johnson, B. B., Moe, P. C., Wang, D., Rossi, K., Trigatti, B. L., Heuck, A. P. (2012) Modifications in Perfringolysin O domain 4 alter the cholesterol concentration threshold required for binding. *Biochemistry* **51**, 3373-3382.

Korchev, Y. E., Bashford, C. L., Pederzolli, C., Pasternak, C.A., Morgan, P. J., Andrew, P. W., Mitchell, T. J. (1998). A conserved tryptophan in pneumolysin is a determinant of the characteristics of channels formed by pneumolysin in cells and planar lipid bilayers. *Biochem J* **329**, 571-7.

Kudryashev, M., Stenta, M., Schmelz, S., Amstutz, M., Wiesand, U., Castano-Diez, D., Degiacomi, M. T., Munnich, S., Bleck, C. K., Kowal, J., Diepold, A., Heinz, D. W., Dal Peraro, M., Cornelis, G. R., and Stahlberg, H. (2013) In situ structural analysis of the Yersinia enterocolitica injectisome. *Elife* **2**, e00792

Liu, S.-L., Sheng, R., Jung, J. H., Wang, L., Stec, E., O'Connor, M. J., Song, S., Bikkavilli, R. K., Winn, R. A., Lee, D., Baek, K., Ueda, K., Levitan, I., Kim, K-P., Cho, W. (2017) Orthogonal lipid sensors identify transbilayer asymmetry of plasma membrane cholesterol. *Nature Chemical Biology*, **13(3),** 268–274.

Maekawa M., Fairn G.D. (2015) Complementary probes reveal that phosphatidylserine is required for the proper transbilayer distribution of cholesterol. *J. Cell Sci*. **128**, 1422–1433.

Maxfield, F. R. & van Meer, G. (2010) Cholesterol, the central lipid of mammalian cells. *Curr. Opin.Cell Biol.* 22**,** 422–429.

Maxfield, F. R. & Tabas, I. (2005) Role of cholesterol and lipid organization in disease. *Nature* **438**, 612-621.

Maxfield, F. R. & Wüstner, D. (2012) Analysis of cholesterol trafficking with fluorescent probes. *Method. Cell Biol.* **108**, 367–393.

Moe, P. C., and Heuck, A. P. (2010) Phospholipid hydrolysis caused by Clostridium perfringens α-toxin facilitates the targeting of perfringolysin O to membrane bilayers. *Biochemistry* **49**, 9498−9507.

Nauth, T., Huschka, F., Shweizer, M., Bosse, J. B., Diepold, A., Failla, A. V., Steffen, A., Stradal, T. E. B., Wolters, M., Aepfelbacher, M. (2018) Visualization of translocons in *Yersinia* type III protein secretion machines during host cell infection. *PloS Pathog.* **14(12)**

Nguyen, V. S. et al. (2015) Structure of AcrH-AopB Chaperone-Translocator Complex Reveals a Role for Membrane Hairpins in Type III Secretion System Translocon Assembly. *Structure* **23**, 2022–2031

Oberley, T. D. and Duncan, J. L. (1971). Characteristics of Streptolysin O. *Infect. Immun* **4(6),** 683-687.

Ohno-Iwashita, Y., Iwamoto, M., Ando, S., and Iwashita, S. (1992) Effect of lipidic factors on membrane cholesterol topology: Mode of binding of θ-toxin to cholesterol in liposomes *Biochim. Biophys. Acta* **1109,** 81– 90.

Park, D., Lara-Tejero, M., Waxham, M. N., Li, W., Hu, B., Galán, J. E., & Liu, J. (2018). Visualization of the type III secretion mediated *Salmonella*-host cell interface using cryo-electron tomography. *eLife*, **7**

Peraro, M. D. and van der Goot, F. G. (2016) Pore-forming toxins: ancient, but never really out of fashion. *Nat. Rev. Microbiol* **14**, 77-92

Pettersson, J., Nordfelth, R., Dubinina, E., Bergman, T., Gustafsson, M., Magnusson, K. E., and Wolf-Watz, H. (1996) Modulation of virulence factor expression by pathogen target cell contact. *Science* **273,** 1231–1233

Sadikot, R. T., Blackwell, T. S., Christman, J. W., and Prince, A. S. (2005) Pathogen-host interactions in Pseudomonas aeruginosa pneumonia. *Am J Respir Crit Care Med* **171**, 1209-1223

Saunders, F.K., Mitchell, T.J., Walker, J.A., Andrew, P.W., Boulnois, G.J. (1989). Pneumolysin, the thiol-activated toxin of Streptococcus pneumoniae, does not require a thiol group for in vitro activity. *Infect. Immun* **57(8),** 2547-52

Savinov, S. N. and Heuck, A. P. (2017). Interaction of Cholesterol with Perfringolysin O: What have we learned from functional analysis? *Toxins* **9***,* 381.

Shatursky, O., Heuck, A. P., Shepard, L. A., Rossjohn, J., Parker, M. W., Johnson, A. E., Tweten, R. K. (1999) The mechanism of membrane insertion for a cholesterol-dependent cytolysin: a novel paradigm for pore-forming toxins. *Cell* **99**, 293–299.

Shepard, L.A., Heuck, A. P., Hamman, B. D., Rossjohn, J., Parker, M. W., Ryan, K. R., Johnson, A. E., Tweten, R. K. (1998) Identification of a Membrane-Spanning Domain of the Thiol-Activated Pore-Forming Toxin Clostridium perfringens Perfringolysin O: An α-Helical to β-Sheet Transition Identified by Fluorescence Spectroscopy. *Biochemistry* **37 (41**), 14563-14574.

Shimada, Y., Maruya, M., Iwashita, S. & Ohno-Iwashita, Y. (2002) The C-terminal domain of perfringolysin O is an essential cholesterol-binding unit targeting to cholesterol-rich microdomains. *Eur. J. Biochem.* **269**, 6195–6203.

Shime, N., Sawa, T., Fujimoto, J., Faure, K., Allmond, L. R., Karaca, T., Swanson, B. L., Spack, E. G., and Wiener-Kronish, J. P. (2001) Therapeutic administration of anti-PcrV F(ab')(2) in sepsis associated with Pseudomonas aeruginosa. *J Immunol* **167**, 5880-5886

Steck, T. L., Lange, Y. (2010) Cell cholesterol homeostasis: Mediation by active cholesterol. *Trends in Cell Biology*. **20(11),** 680-687.

Ramachandran, R., Tweten, R.K., Johnson, A. E. (2004) Membrane-dependent conformational changes initiate cholesterol-dependent cytolysin oligomerization and intersubunit β-strand alignment. *Nat. Struct. Mol. Biol*., **11**, 697-705.

Ramachandran, R., Heuck, A.P., Tweten, R.K. Johnson, A.E. (2002) Structural insights into the membrane-anchoring mechanism of a cholesterol-dependent cytolysin. *Nat. Struct. Biol*. **9**, 823-827.

Ramirez-Estrada, S., Borgatta, B., and Rello, J. (2016) Pseudomonas aeruginosa ventilator-associated pneumonia management. *Infect Drug Resist* **9**, 7-18

Romano, F. B., Rossi, K. C., Savva, C. G., Holzenburg, A., Clerico, E. M., and Heuck, A. P. (2011) Efficient isolation of *Pseudomonas aeruginosa* type III secretion translocators and assembly of heteromeric transmembrane pores in model membranes.Biochemistry **50**, 7117–7131

Romano, F. B., Tang, Y., Rossi, K. C., Monopoli, K. R., Ross, J. L., and Heuck, A. P. (2016) Type 3 Secretion Translocators Spontaneously Assemble a Hexadecameric Transmembrane Complex. *J. Biol. Chem*. **291**, 6304-6315

Rossjohn J., Feil, S.C., McKinstry, W.J., Tweten, R.K., Parker, M.W. (1997) Structure of a cholesterol-binding thiol-activated cytolysin and a model of its membrane form. *Cell*, **89,** 685-692

Tang, Y. (2018) Studies on the P. aeruginosa T3S translocon assembly: interaction of PopD with membranes. *Doctoral Dissertations*. 1296.

Tang, Y., Romano, F. B., Breña, M., Heuck, A. P. (2018) The Pseudomonas aeruginosa type III secretion translocator PopB assists the insertion of translocator PopD into cell membranes. *J. Biol. Chem*. **293(23),** 8982-8993

Vallis, A. J., T. L. Yahr, J. T. Barbieri, and D. W. Frank. (1999) Regulation of ExoS production and secretion by Pseudomonas aeruginosa in response to tissue culture conditions. *Infect. Immun*. **67**, 914-920

Vermeulen A.J., Tang Y., Heuck A.P. (2016) Translocation of Toxins by Gram Negative Pathogens Using the Type III Secretion System. *Microbial Toxins, Toxinology*

Worrall, L. J., Hong, C., Vuckovic, M., Deng, W., Bergeron, J. R., Majewski, D. D., Huang, R. K., Spreter, T., Finlay, B. B., Yu, Z., and Strynadka, N. C. (2016) Near-atomic-resolution cryo-EM analysis of the Salmonella T3S injectisome basal body. *Nature* **540**, 597-601

Yin, J., Straight, P. D., McLoughlin, S. M., Zhou, Z., Lin, A. J., Golan, D. E., Kelleher, N. L., Kolter, R., Walsh, C. T. (2005) Genetically encoded short peptide tag for versatile protein labeling by Sfp phosphopantetheinyl transferase. *PNAS*. **102 (44)** 15815-15820